

FTUAM 07/01
IFT-UAM/CSIC-07-02
HIP-2006-02/TH
LPT-ORSAY-07-02
hep-ph/0701271

31 January 2007

Phenomenological viability of neutralino dark matter in the NMSSM

D. G. Cerdeño ^{a,b}, E. Gabrielli ^c, D. E. López-Fogliani ^{a,b}, C. Muñoz ^{a,b}, A. M. Teixeira ^d

^a*Departamento de Física Teórica C-XI, Universidad Autónoma de Madrid, Cantoblanco, E-28049 Madrid, Spain*

^b*Instituto de Física Teórica C-XVI, Universidad Autónoma de Madrid, Cantoblanco, E-28049 Madrid, Spain*

^c*Helsinki Institute of Physics P.O.B 64, 00014 University of Helsinki, Finland*

^d*Laboratoire de Physique Théorique, Université de Paris-Sud XI, Bâtiment 201, F-91405 Orsay Cedex, France*

Abstract

The viability of the lightest neutralino as a dark matter candidate in the Next-to-Minimal Supersymmetric Standard Model is analysed. We carry out a thorough analysis of the parameter space, taking into account accelerator constraints as well as bounds on low-energy observables, such as the muon anomalous magnetic moment and rare K and B meson decays. The neutralino relic density is also evaluated and consistency with present bounds imposed. Finally, the neutralino direct detection cross section is calculated in the allowed regions of the parameter space and compared to the sensitivities of present and projected dark matter experiments. Regions of the parameter space are found where experimental constraints are fulfilled, the lightest neutralino has the correct relic abundance and its detection cross section is within the reach of dark matter detectors. This is possible in the presence of very light singlet-like Higgses and when the neutralino is either light enough so that some annihilation channels are kinematically forbidden, or has a large singlino component.

PACS: 12.60.Jv, 95.35.+d

1 Introduction

One of the most interesting candidates for dark matter, within the class of Weakly Interactive Massive Particles (WIMPs), is the lightest neutralino ($\tilde{\chi}_1^0$), which arises in the context of R-parity conserving supersymmetric (SUSY) models [1]. Although neutralino dark matter has been extensively examined in the framework of the Minimal Supersymmetric Standard Model (MSSM) [2], this is not the case of the Next-to-Minimal Supersymmetric Standard Model (NMSSM) [3].

The NMSSM is an extension of the MSSM by a singlet superfield S , which provides an elegant solution to the so-called μ problem of the MSSM [4]. In this case, an effective μ term is dynamically generated when the scalar component of S acquires a vacuum expectation value (VEV) of order of the SUSY breaking scale. In addition, and when compared to the MSSM, the NMSSM renders less severe the “little fine tuning problem” of the MSSM [5], or equivalently, the non-observation of a neutral CP-even Higgs boson at LEP II. The presence of additional fields, namely an extra CP-even and CP-odd neutral Higgs bosons, as well as a fifth neutralino, leads to a richer and more complex phenomenology [6–10]. In particular, a very light neutralino may be present [7]. The upper bound on the mass of the lightest Higgs state is larger than in the MSSM [8]. Moreover, a very light Higgs boson is not experimentally excluded. All these properties also contribute to the emergence of dark matter scenarios that can be very different from those encountered in the MSSM, both regarding the relic density and the prospects for direct detection.

The NMSSM must comply with a large number of experimental constraints. In addition to LEP II and Tevatron limits on the spectrum, one should also take into account SUSY contributions to low-energy observables. The most stringent bounds arise from kaon and B decays, as well as from the muon anomalous magnetic moment, a_μ^{SUSY} . Naturally, in order to be a viable dark matter candidate, the NMSSM lightest neutralino must also satisfy the present astrophysical bounds on the relic abundance. It is important to notice that, in addition to the channels already present in the MSSM, the NMSSM offers new kinematically viable annihilation channels and potential resonances [11–13], due to the presence of light scalar and pseudoscalar Higgses.

The direct detection of neutralino dark matter has been discussed in the framework of the NMSSM in Refs. [13–16]. In particular, and as pointed out in [16], the exchange of very light Higgses can lead to large direct detection cross sections, within the reach of the present generation of dark matter detectors. There are currently a large number

of facilities devoted to the direct detection of WIMPs through their elastic scattering with nuclei. Among them, it is important to refer to the DAMA collaboration [17, 18] (which has already reported data favouring the existence of a WIMP signal¹), CDMS Soudan [20], EDELWEISS [21] and ZEPLIN I [22], as well as the upcoming detectors working with 1 tonne of Ge/Xe [23].

The purpose of the present work is to extend the analysis of Ref. [16]. In addition to upgrading the experimental constraints already present in the previous work, we now include the computation of the SUSY contribution to the muon anomalous magnetic moment, and bounds from K - and B -meson decays. Moreover, we incorporate the evaluation of the relic abundance of the lightest neutralino in the NMSSM.

Our work is organised as follows. We briefly address the most relevant aspects of the NMSSM in Section 2, paying especial attention to the minimisation of the Higgs potential and to the new features of the Higgs and neutralino sectors. We also comment on the various constraints on the low-energy observables that will be included in the analysis. In Section 3 we introduce the NMSSM lightest neutralino as a dark matter candidate and discuss the potential implications regarding its detection cross section and relic abundance. Our results are presented in Section 4, where we first analyse the effect of the experimental constraints on low-energy observables, a_μ^{SUSY} and $b \rightarrow s\gamma$, on the parameter space (Sec. 4.1). We then include the constraint on the neutralino relic density (Sec. 4.2). Finally, taking all these bounds into account, we evaluate the neutralino detection cross section on the allowed regions of the parameter space (Sec. 4.3), comparing the results with the sensitivity of dark matter detectors. We summarise our conclusions in Section 5.

2 The low-energy NMSSM

In this section we briefly review some of the most relevant aspects of the NMSSM, and summarise the main constraints considered when analysing the parameter space.

¹Notice that the DAMA result has not been confirmed by the other experiments. For attempts to show that DAMA and these experiments might not be in conflict, see Ref. [19].

2.1 Overview of the model

With the addition of a gauge singlet superfield, the MSSM superpotential is modified as follows:

$$W = \epsilon_{ij} (Y_u H_2^j Q^i u + Y_d H_1^i Q^j d + Y_e H_1^i L^j e) - \epsilon_{ij} \lambda S H_1^i H_2^j + \frac{1}{3} \kappa S^3, \quad (2.1)$$

where $H_1^T = (H_1^0, H_1^-)$, $H_2^T = (H_2^+, H_2^0)$, i, j are $SU(2)$ indices, and $\epsilon_{12} = 1$. In this model, the usual MSSM bilinear μ term is absent from the superpotential, and only dimensionless trilinear couplings are present in W . However, when the scalar component of S acquires a VEV, an effective interaction $\mu H_1 H_2$ is generated, with $\mu \equiv \lambda \langle S \rangle$. Likewise, the soft SUSY breaking terms are accordingly modified, so to include new soft-breaking masses for the singlet (m_S^2), and additional trilinear couplings (A_λ and A_κ). After electroweak (EW) symmetry is spontaneously broken, the neutral Higgs scalars develop the following VEVs:

$$\langle H_1^0 \rangle = v_1, \quad \langle H_2^0 \rangle = v_2, \quad \langle S \rangle = s. \quad (2.2)$$

After computing the tree-level scalar potential², $V_{\text{neutral}}^{\text{Higgs}}$, one must ensure the presence of a true minimum. The minimisation can be conveniently separated into two steps. First, one imposes a minimum of $V_{\text{neutral}}^{\text{Higgs}}$ with respect to the phases (signs) of the VEVs, while in a later stage one derives the conditions regarding the modulus of the VEVs. The first step immediately allows to directly exclude combinations of signs for the parameters. In fact, and working under the convention where λ and $\tan \beta$ are positive, and κ , $\mu (= \lambda s)$, A_λ and A_κ can have both signs, one can analytically show that there are only four distinct combinations of signs for κ , A_λ , A_κ , and μ that ensure the presence of a minimum of $V_{\text{neutral}}^{\text{Higgs}}$ [16]:

(i) $\kappa > 0$, $\text{sign}(s) = \text{sign}(A_\lambda) = -\text{sign}(A_\kappa)$,

which always leads to a minimum with respect to the phases of the VEVs.

(ii) $\kappa > 0$, $\text{sign}(s) = -\text{sign}(A_\lambda) = -\text{sign}(A_\kappa)$,

with $|A_\kappa| > 3\lambda v_1 v_2 |A_\lambda| / (-|s A_\lambda| + \kappa |s^2|)$, where the denominator has to be positive.

(iii) $\kappa > 0$, $\text{sign}(s) = \text{sign}(A_\lambda) = \text{sign}(A_\kappa)$,

with $|A_\kappa| < 3\lambda v_1 v_2 |A_\lambda| / (|s A_\lambda| + \kappa |s^2|)$.

²For details about the Lagrangian and the neutral Higgs potential, $V_{\text{neutral}}^{\text{Higgs}}$, of the model see Ref. [16].

(iv) $\kappa < 0$, $\text{sign}(s) = \text{sign}(A_\lambda) = \text{sign}(A_\kappa)$,

with $|A_\kappa| > 3\lambda v_1 v_2 |A_\lambda| / (|sA_\lambda| - \kappa|s^2|)$, where the denominator has to be positive.

The additional conditions regarding the minimisation of the potential with respect to the Higgs VEVs can be derived, and these allow to re-express the soft breaking Higgs masses in terms of λ , κ , A_λ , A_κ , v_1 , v_2 and s :

$$\begin{aligned} m_{H_1}^2 &= -\lambda^2 (s^2 + v^2 \sin^2 \beta) - \frac{1}{2} M_Z^2 \cos 2\beta + \lambda s \tan \beta (\kappa s + A_\lambda) , \\ m_{H_2}^2 &= -\lambda^2 (s^2 + v^2 \cos^2 \beta) + \frac{1}{2} M_Z^2 \cos 2\beta + \lambda s \cot \beta (\kappa s + A_\lambda) , \\ m_S^2 &= -\lambda^2 v^2 - 2\kappa^2 s^2 + \lambda \kappa v^2 \sin 2\beta + \frac{\lambda A_\lambda v^2}{2s} \sin 2\beta - \kappa A_\kappa s , \end{aligned} \quad (2.3)$$

where $v^2 = v_1^2 + v_2^2 = 2M_W^2/g_2^2$ and $\tan \beta = v_2/v_1$.

The neutral Higgs spectrum in the NMSSM includes three scalars, and two pseudoscalar states, whose mass matrices have been discussed in [16]. For our present analysis, let us just recall that in either case interaction and physical eigenstates can be related as

$$h_a^0 = S_{ab} H_b^0 \quad (a, b = 1\dots 3), \quad a_i^0 = P_{ij} P_j^0 \quad (i, j = 1, 2), \quad (2.4)$$

where S (P) is the unitary matrix that diagonalises the 3×3 (2×2) scalar (pseudoscalar) Higgs mass matrix. In both sectors, we order the physical eigenstates as $m_{h_1^0} \lesssim m_{h_2^0} \lesssim m_{h_3^0}$ and $m_{a_1^0} \lesssim m_{a_2^0}$. The singlet component of the lightest CP-even Higgs is therefore given by S_{13} .

A final comment concerns the neutralino sector, now extended to include the singlino component of the new chiral superfield, S . In the weak interaction basis defined by $\Psi^{0T} \equiv (\tilde{B}^0 = -i\lambda', \tilde{W}_3^0 = -i\lambda_3, \tilde{H}_1^0, \tilde{H}_2^0, \tilde{S})$ the neutralino mass matrix reads

$$\mathcal{M}_{\tilde{\chi}^0} = \begin{pmatrix} M_1 & 0 & -M_Z \sin \theta_W \cos \beta & M_Z \sin \theta_W \sin \beta & 0 \\ 0 & M_2 & M_Z \cos \theta_W \cos \beta & -M_Z \cos \theta_W \sin \beta & 0 \\ -M_Z \sin \theta_W \cos \beta & M_Z \cos \theta_W \cos \beta & 0 & -\lambda s & -\lambda v_2 \\ M_Z \sin \theta_W \sin \beta & -M_Z \cos \theta_W \sin \beta & -\lambda s & 0 & -\lambda v_1 \\ 0 & 0 & -\lambda v_2 & -\lambda v_1 & 2\kappa s \end{pmatrix}. \quad (2.5)$$

The above matrix can be diagonalised by means of a unitary matrix N ,

$$N^* \mathcal{M}_{\tilde{\chi}^0} N^{-1} = \text{diag}(m_{\tilde{\chi}_1^0}, m_{\tilde{\chi}_2^0}, m_{\tilde{\chi}_3^0}, m_{\tilde{\chi}_4^0}, m_{\tilde{\chi}_5^0}), \quad (2.6)$$

where $m_{\tilde{\chi}_1^0}$ is the lightest neutralino mass. Under the above assumptions, the lightest neutralino can be expressed as the combination

$$\tilde{\chi}_1^0 = N_{11} \tilde{B}^0 + N_{12} \tilde{W}_3^0 + N_{13} \tilde{H}_1^0 + N_{14} \tilde{H}_2^0 + N_{15} \tilde{S}. \quad (2.7)$$

In the following, neutralinos with $N_{13}^2 + N_{14}^2 > 0.9$, or $N_{15}^2 > 0.9$, will be referred to as Higgsino- or singlino-like, respectively.

2.2 Constraints on the parameter space

In addition to ensuring the presence of a minimum of the potential, other constraints, both theoretical and experimental, must be imposed on the parameter space generated by the low-energy NMSSM degrees of freedom

$$\lambda, \kappa, \tan\beta, \mu, A_\lambda, A_\kappa. \quad (2.8)$$

The soft supersymmetry-breaking terms, namely gaugino masses, $M_{1,2,3}$, scalar masses, $m_{Q,L,U,D,E}$, and trilinear parameters, $A_{Q,L,U,D,E}$, are also taken as free parameters and specified at low scale.

A comprehensive analysis of the low-energy NMSSM phenomenology can be obtained using the NMHDECAY 2.0 code [24]. After minimising the scalar potential, thus dismissing the presence of tachyons and/or false minima, the Higgs boson masses are computed, including 1- and 2-loop radiative corrections. Squark and slepton masses are also calculated, as well as the corresponding mixing angles for the third generation. Chargino and neutralino masses and mixings are evaluated and all the relevant couplings are derived.

Even though the general analysis is performed at low-energy, a further theoretical constraint can be derived, namely the absence of a Landau pole for λ , κ , Y_t and Y_b below the GUT scale. Including logarithmic one-loop corrections to λ and κ , the latter constraint translates into $\lambda \lesssim 0.75$, $|\kappa| \lesssim 0.65$, with $1.7 \lesssim \tan\beta \lesssim 54$.

On the experimental side, NMHDECAY 2.0 includes accelerator (LEP and Tevatron) constraints, B -meson decays, and dark matter relic density through a link to micrOMEGAS [25]. In particular, direct bounds on the masses of the charged particles (H^\pm , $\tilde{\chi}^\pm$, \tilde{q} , \tilde{l}) and on the gluino mass are taken into account [26, 27]. Excessive contributions to the invisible decay width of the Z boson [28, 29], as those potentially arising from $Z \rightarrow \tilde{\chi}_i^0 \tilde{\chi}_j^0$ and $Z \rightarrow h^0 a^0$, are also excluded from the parameter space. Finally, in the neutral Higgs sector, one checks the constraints on the production rates for all the CP-even states h^0 and CP-odd states a^0 , in all the channels studied at LEP [30]: $e^+e^- \rightarrow h^0 Z$, independent of the h^0 decay mode (IHDM); $e^+e^- \rightarrow h^0 Z$, dependent on the h^0 decay mode (DHDM), with the Higgs decaying via $h^0 \rightarrow b\bar{b}$, $h^0 \rightarrow \tau^+\tau^-$, $h^0 \rightarrow 2\text{jets}$ $h^0 \rightarrow \gamma\gamma$ and $h^0 \rightarrow \text{invisible}$; associated production modes

(APM), $e^+e^- \rightarrow h^0a^0$, with $h^0a^0 \rightarrow 4b$'s, $h^0a^0 \rightarrow 4\tau$'s and $h^0a^0 \rightarrow a^0a^0a^0 \rightarrow 6b$'s. In addition to the latter, one also takes into account the possible two body decays of all CP-even, CP-odd and charged Higgs bosons into squarks and sleptons, as well as radiatively induced decays of neutral Higgs bosons into two photons and two gluons.

Regarding B -meson decays, and although the NMHDECAY 2.0 code already contains a rough estimate of the $b \rightarrow s\gamma$ decay branching ratio (evaluated at the leading order in QCD), we include in our code a more precise computation of the $b \rightarrow s\gamma$ decay in the NMSSM [31], taking into account next-to-leading order (NLO) contributions [32, 33], following the results of [34]. However, we only include leading order (LO) SUSY contributions to the Wilson coefficients at the M_W scale³. The calculation within the context of the MSSM at LO and NLO can be found in [35] and [36], respectively. The most recent experimental world average for the branching ratio (BR) reported by the Heavy Flavour Averaging Group is [28, 37]

$$\text{BR}^{\text{exp}}(b \rightarrow s\gamma) = (3.55 \pm 0.27) \times 10^{-4}. \quad (2.9)$$

On the other hand, the current SM prediction for the branching ratio is [38]

$$\text{BR}^{\text{SM}}(b \rightarrow s\gamma) = (3.73 \pm 0.30) \times 10^{-4}, \quad (2.10)$$

where the charm-loop contribution has been included [33]. We have estimated the theoretical error that results from varying the scales in the $b \rightarrow s\gamma$ calculation within the NMSSM, following the method described in [34]. We add to this the experimental error in quadrature. This procedure is performed at every point of the parameter space, typically leading to an error of about 10% of the total $\text{BR}(b \rightarrow s\gamma)$ value. Consistency at 2σ with the experimental central value of Eq. (2.9) is then demanded.

We have also included in our code other constraints coming from the contribution of a light pseudoscalar a^0 in NMSSM to the rare B - and K -meson decays [31]. When the pseudoscalar is very light it could be produced in meson decays and significantly affect the rates for $K - \bar{K}$ and $B - \bar{B}$ mixing and other SM decays. In particular, our code takes into account the constraints from the pseudo-scalar indirect contributions to $K - \bar{K}$ and $B - \bar{B}$ mixing, $B \rightarrow \mu^+\mu^-$, $B \rightarrow X_s\mu^+\mu^-$, $B^- \rightarrow K^-\nu\bar{\nu}$, $B \rightarrow K_S^0X^0$,

³No charm-loop contributions were included in the analysis of Ref. [34], giving a SM central value of $\text{BR}^{\text{SM}}(b \rightarrow s\gamma) = 3.293 \times 10^{-4}$. This result is obtained by extrapolating the value of the branching ratio evaluated at $\delta = 0.9$ and $\mu_b = m_b$, where δ parameterises the photon energy cut $E_\gamma > (1-\delta)m_b/2$ and μ_b is the renormalisation scale. The corresponding new physics contribution has been implemented in our code by using the parameterisation of [34] evaluated at $\mu_b = m_b$ and $\delta = 0.9$.

and by the direct production, at large $\tan\beta$, via $b \rightarrow sa^0$, $B \rightarrow Ka^0$, and $B \rightarrow \pi a^0$ decays.

Finally, in our analysis we will also include the constraints coming from the SUSY contributions to the muon anomalous magnetic moment, $a_\mu = (g_\mu - 2)$ [39]. Taking into account the most recent theoretical predictions for this quantity within the SM [40–42] and the measured experimental value [43], the observed excess in a_μ^{exp} constrains a possible supersymmetric contribution to be $a_\mu^{\text{SUSY}} = (27.6 \pm 8) \times 10^{-10}$, where theoretical and experimental errors have been combined in quadrature.

The evaluation of a_μ^{SUSY} in the NMSSM has been included in our analysis, and consistency at the 2σ level imposed. Thus those regions of the parameter space not fulfilling $11.6 \times 10^{-10} \lesssim a_\mu^{\text{SUSY}} \lesssim 43.6 \times 10^{-10}$ will be considered disfavoured.

3 Dark matter in the NMSSM

The new features of the NMSSM have an impact on the properties of the lightest neutralino as a dark matter candidate, affecting both its direct detection and relic abundance.

The computation of the spin-independent part of the neutralino-nucleon cross section was discussed in detail in [16]. It was pointed out there that the existence of a fifth neutralino state, together with the presence of new terms in the Higgs-neutralino-neutralino interaction (which are proportional to λ and κ), trigger new contributions to the spin-independent part of the neutralino-nucleon cross section, $\sigma_{\tilde{\chi}_1^0-p}$. On the one hand, although the term associated with the s -channel squark exchange is formally identical to the MSSM case, it can be significantly reduced if the lightest neutralino has a major singlino composition. On the other hand, and more importantly, the dominant contribution to $\sigma_{\tilde{\chi}_1^0-p}$, associated to the exchange of CP-even Higgs bosons on the t -channel can be largely enhanced when these are very light. In the NMSSM, the lightest CP-even Higgs can escape detection if its singlet composition is large. For instance, this makes possible the presence of scenarios with $m_{h_1^0} \lesssim 70$ GeV, thus considerably enhancing the neutralino-nucleon interaction. Consequently, large detection cross sections can be obtained, even within the reach of the present generation of dark matter detectors.

However, in order to be a good dark matter candidate, the lightest NMSSM neutralino must also comply with the increasingly stringent bounds on its relic density.

Astrophysical constraints, stemming from the analysis of galactic rotation curves [44], clusters of galaxies and large scale flows [45], suggest the following range for the WIMP relic abundance

$$0.1 \lesssim \Omega h^2 \lesssim 0.3, \quad (3.11)$$

which can be further reduced to

$$0.095 \lesssim \Omega h^2 \lesssim 0.112, \quad (3.12)$$

taking into account the recent three years data from the WMAP satellite [46].

Compared to what occurs in the MSSM, one would expect several alterations regarding the dominant processes. As discussed in [13], and as mentioned above regarding the direct detection cross section, the differences can be present at distinct levels. First, and given the presence of a fifth neutralino (singlino), the composition of the annihilating WIMPs can be significantly different from that of the MSSM in wide regions of the parameter space. Having the possibility of a singlino-like lightest supersymmetric particle (LSP), associated with the presence of new couplings in the interaction Lagrangian, in turn favours the coupling of the WIMPs to a singlet-like Higgs, whose mass can be substantially lighter than in the MSSM, given the more relaxed experimental constraints. Regarding the channels through which neutralino annihilation occurs, in the NMSSM we have new open channels, essentially due to the existence of light Higgs states. In summary, the presence of additional Higgs states (scalar and pseudoscalar) favours annihilation via s -channel resonances. On the other hand, having light h_1^0 and a_1^0 states that are experimentally viable means that new channels with annihilation into $Z h_1^0$, $h_1^0 h_1^0$, $h_1^0 a_1^0$ and $a_1^0 a_1^0$ (either via s -channel Z , h_i^0 , a_i^0 exchange or t -channel neutralino exchange) can provide important contributions to the annihilation and co-annihilation cross-sections [12].

Noticing that important annihilation channels (s -channel) are related to the t -channel processes responsible for the most relevant contributions to $\sigma_{\tilde{\chi}_1^0-p}$, one should expect a strong interplay between a viable relic density, and promising prospects for the direct detection of the NMSSM dark matter candidate. In fact, there should be regions of the parameter space which provide new and interesting scenarios⁴.

⁴As concluded in [13], it might even be possible to reconcile a very light neutralino with the experimental observations from DAMA, CDMS II, and WMAP.

4 Results and discussion

In this section, we study the viability of lightest NMSSM neutralino as a good dark matter candidate. Motivated by the results obtained in [16], we focus on regions of the low-energy NMSSM parameter space where large direct detection cross sections are likely to be obtained. Building upon the previous analysis, we apply the new constraints (improved comparison with LEP and Tevatron data), K - and B -meson decays, a_μ^{SUSY} , and compatibility with the WIMP relic density. Finally, we discuss the prospects of the experimentally viable regions regarding direct detection of dark matter.

Let us just recall that the free parameters of the model, associated with the Higgs and neutralino sectors of the theory, are ⁵

$$\lambda, \quad \kappa, \quad \mu(= \lambda s), \quad \tan \beta, \quad A_\lambda, \quad A_\kappa, \quad M_1, \quad M_2, \quad M_3. \quad (4.13)$$

We assume that the gaugino mass parameters mimic, at low-energy, the values of a hypothetical GUT unification ($\frac{M_3}{6} = M_1 = \frac{M_2}{2}$).

It should be emphasised that in NMHDECAY 2.0 some of the input parameters are specified at a different scale than in the former version NMHDECAY 1.1 [9], which was used in the previous analysis [16]. Although the difference between the values of λ (or κ) at the EW and the SUSY scales (≈ 1 TeV) is very small, there is a substantial change in the value of the trilinear coupling A_λ . These variations are induced by the top trilinear coupling A_{top} , and are approximately given by $A_\lambda^{\text{SUSY}} \approx A_\lambda^{\text{EW}} + A_{\text{top}}^{\text{EW}}$. Therefore, one needs to take this shift into account when comparing the present results with those of [16].

Motivated by the results of [16] regarding the prospects for direct detection of dark matter, we will be interested in a regime of low $\tan \beta$, as well as in values of $|\mu|$ in the range $110 \text{ GeV} \lesssim \mu \lesssim 200 \text{ GeV}$ (the lower limit ensuring that in most cases one can safely avoid the LEP bound on the lightest chargino mass). Likewise, the following intervals for the trilinear couplings will be taken: $-800 \text{ GeV} \lesssim A_\lambda \lesssim 800 \text{ GeV}$, and $-300 \text{ GeV} \lesssim A_\kappa \lesssim 300 \text{ GeV}$ (the optimal ranges will typically correspond to $|A_\lambda| \sim 400 \text{ GeV}$ and $|A_\kappa| \lesssim 200 \text{ GeV}$, working in a small $\tan \beta$ regime).

Slepton and squark masses, as well as the corresponding trilinear parameters, do not significantly affect the neutralino detection properties, other than through the

⁵Although the soft gluino mass, M_3 , is not directly related to the computation of the Higgs/neutralino masses and mixings, it plays a relevant role in contributing to the radiative corrections to the Higgs boson masses.

radiative corrections to the Higgs masses. However, low-energy observables are very sensitive to their specific values. In the following section we will see, for instance, how the experimental constraint on a_μ^{SUSY} favours light sleptons.

As already done in Ref. [16], we divide the scan of the low-energy NMSSM parameter space following the results of the minimisation with respect to the VEV phases, separately discussing each of the cases (i)-(iv) (see Section 2.1).

4.1 NMSSM parameter space: updated constraints

We first discuss the new constraints on the parameter space arising from the improved analysis on the Higgs sector, the muon anomalous magnetic moment, and K - and B -meson decays.

Among the new features implemented in NMHDECAY 2.0, one finds additional radiative corrections to the Higgs boson masses, including corrections of order $g^2 Y_{t,b}^2$ to the CP-even Higgs boson mass (induced by stop/sbottom D -term couplings). Regarding the logarithmic one-loop corrections of the order g^2 , these are now dependent on the different masses of squarks/sleptons of distinct generations. Moreover, the corrections to fourth order in λ and κ are also taken into account. The computation of the sparticle spectrum is also complete in the new version, and all squark and gluino data is confronted with the constraints from both Tevatron and LEP. With respect to the results obtained in the previous analysis [16], the latter improvements only translate into slight changes in the exclusion regions.

Concerning the evaluation of the supersymmetric contributions to the muon anomalous magnetic moment, the relevant processes comprise neutralino-sneutrino as well as chargino-smuon loops. The only change with respect to the MSSM is due to the fifth neutralino state and the corresponding modified neutralino-lepton-slepton coupling. Since we are interested in cases with very low $\tan\beta$, the contributions from neutralino and chargino loops are of similar magnitude, and very small. For example, with $\tan\beta = 3$ and slepton mass parameters above $m_{E,L} \sim 1$ TeV one typically obtains $a_\mu^{\text{SUSY}} \sim 10^{-11}$, which is disfavoured. In order to obtain compatibility with the experimental result an increase in the value of $\tan\beta$ is welcome, but this would then lead to regions of the parameter space where, from the dark matter point of view, the NMSSM resembles the MSSM. The other possibility is decreasing the slepton (and gaugino) masses. Furthermore, large values of the slepton trilinear couplings are needed in order to increase the LR mixing in the smuon mass matrix. The choice $\mu A_E < 0$ is

optimal, since it makes the neutralino contribution positive and large. For example, with $\tan\beta \sim 5$, $A_E = -2500$ GeV and $m_{E,L} \lesssim 200$ GeV, one obtains $a_\mu^{\text{SUSY}} \gtrsim 10^{-9}$ for $M_1 \lesssim 215$ GeV. The relevance of these changes is illustrated in Fig. 1, where the numerical results for a_μ^{SUSY} are plotted versus the bino mass, M_1 , for different combinations of slepton mass and trilinear couplings. For each case we have also varied A_λ and A_κ over a wide range and scanned the whole (λ, κ) plane, which as evidenced in the figure has virtually no effect on the resulting a_μ^{SUSY} . We have also included the various LEP and Tevatron constraints. For the rest of our analysis, we will assume $m_{E,L} = 150$ GeV and $A_E = -2500$ GeV. Also, and unless otherwise stated, we will set the bino mass to $M_1 = 160$ GeV, which, according to Fig. 1, leads to a sufficiently large a_μ^{SUSY} . The detection properties of the neutralino are in general quite insensitive to changes in the slepton sector. Notice however that if one does not wish to impose the bound on the muon anomalous magnetic moment, heavy sleptons (equal to squarks) can be taken which would not affect the dark matter predictions.

Regarding the bounds arising from K - and B -meson physics, the most important role is played by the $b \rightarrow s \gamma$ decay, which can in principle exclude important regions of the parameter space. Concerning the other K - and B -meson processes discussed in Section 2.2, we have verified that throughout the investigated NMSSM parameter space they are always in good agreement with experiment, so that we will make no further reference to the latter in the following discussion of the numerical results.

In the present analysis we will not take into account any source of flavour violation other than the Cabibbo-Kobayashi-Maskawa (CKM) matrix. Moreover, we will be systematically considering large values for the gluino mass (above 1 TeV). Under the latter assumptions, the most important contributions to $\text{BR}(b \rightarrow s \gamma)$ arise in general from charged Higgs and chargino mediated diagrams [35].

On the one hand, when the dominant contributions are those stemming from charged Higgs exchange, the results for $\text{BR}(b \rightarrow s \gamma)$ closely follow the behaviour of the charged Higgs mass, which in the NMSSM is given by

$$m_{H^\pm}^2 = \frac{2\mu^2}{\sin(2\beta)} \frac{\kappa}{\lambda} - v^2 \lambda^2 + \frac{2\mu A_\lambda}{\sin(2\beta)} + M_W^2. \quad (4.14)$$

From the above, we expect that smaller values of $\text{BR}(b \rightarrow s \gamma)$ should be obtained for large $m_{H^\pm}^2$, and therefore when κ/λ is sizable (for positive values of κ) or for small κ/λ (if $\kappa < 0$). In general, smaller values of the $\text{BR}(b \rightarrow s \gamma)$ will be also associated to larger values of the product μA_λ . Furthermore, the leading term of the Wilson coefficient associated to the charged Higgs varies as $\tan^{-2}\beta$ [35]. As a consequence,

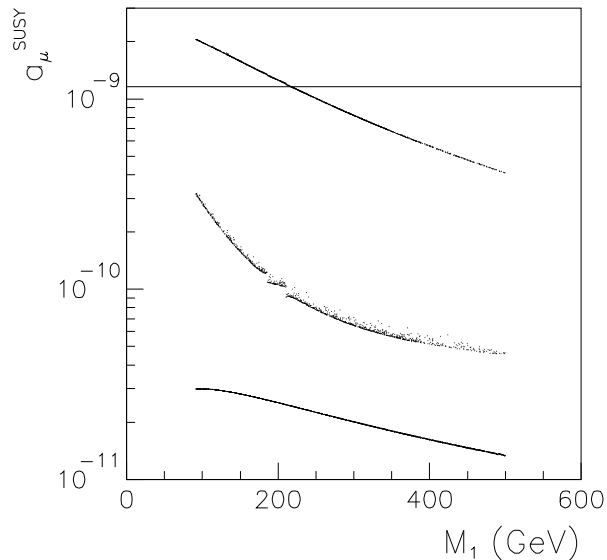


Figure 1: Supersymmetric contribution to the anomalous magnetic moment of the muon as a function of the bino mass, M_1 , for $\tan\beta = 5$, $\mu = 150$ GeV, trilinear couplings in the range $-800 \lesssim A_\lambda \lesssim 800$ GeV, $-300 \lesssim A_\kappa \lesssim 300$ GeV. From bottom to top, the different bands correspond to the following values of the slepton mass and lepton trilinear terms, $m_{L,E} = 1$ TeV with $A_E = 1$ TeV, $m_{L,E} = 150$ GeV with $A_E = 1$ TeV, and $m_{L,E} = 150$ GeV with $A_E = -2.5$ TeV. A full scan on the (λ, κ) plane has been performed for each case, including LEP and Tevatron experimental constraints. The horizontal solid line indicates the lower bound of the allowed 2σ interval.

one expects a decrease of this contribution as $\tan\beta$ increases. On the other hand, in a regime of $\mu \lesssim M_2$, the lightest chargino is Higgsino-dominated, so that its mass is also quite small ($m_{\tilde{\chi}_1^\pm} \sim \mu$). Thus, the chargino contributions (which are opposite in sign to those of the charged Higgs) are also expected to play a relevant role, although, in the cases analysed in this paper ($\tan\beta \lesssim 10$), they are not dominant. Gluino contributions are also very small, given the little flavour violation in the down squark sector, and the sizable values of M_3 . Likewise, neutralino exchange contributions are almost negligible. We thus find that, in general, the NMSSM contribution to $\text{BR}(b \rightarrow s \gamma)$ at low $\tan\beta$ is large and mostly arising from charged Higgs loops. This leads to stringent constraints on the parameter space.

Let us study the effect of the experimental bound on $\text{BR}(b \rightarrow s \gamma)$, together with the updated accelerator constraints on the NMSSM parameter space. After this first survey we will no longer separately address the K - and B -meson constraints (and

a_μ) from those arising from LEP/Tevatron data. Henceforth, experimentally allowed regions will be those that not only comply with the latter data, but that also exhibit $\text{BR}(b \rightarrow s \gamma)$ within 2σ from its central experimental value. As mentioned before, in order to satisfy the constraint on the muon anomalous magnetic moment, we take $M_1 = 160$ GeV in the following subsection, for which, in the case with $\tan\beta = 5$, $a_\mu^{\text{SUSY}} \approx 1.4 \times 10^{-9}$ (see Fig. 1).

4.1.1 $\mu A_\kappa < 0$ and $\mu A_\lambda > 0$ ($\kappa > 0$)

As discussed in [16], this is one of the most interesting areas of the parameter space, since although sizable regions are excluded due to the occurrence of tachyons in the CP-even Higgs sector (namely for larger values of $|A_\kappa|$), the possibility of having experimentally viable light scalar Higgs leads to potentially large values for $\sigma_{\tilde{\chi}_1^0-p}$.

As an example, we represent on the left-hand side of Fig. 2 the (λ, κ) parameter space for an example with $\tan\beta = 3$, $A_\lambda = 200$ GeV, $A_\kappa = -200$ GeV and $\mu = 130$ GeV. The tachyonic region in the CP-even Higgs sector is depicted, as well as the region excluded due to the presence of false minima of the potential. An important part of the theoretically allowed region is also ruled out due to conflict with LEP and/or Tevatron data. This owes to the fact that the doublet component of the lightest scalar Higgs is very large and gives rise to excessive Higgs production rates, in particular, $e^+e^- \rightarrow h^0 Z$, IDHM and DHDM ($h^0 \rightarrow b\bar{b}$ and to a lesser extent, $h^0 \rightarrow 2$ jets). Once all these bounds are applied, a small area on the right of that experimentally excluded survives, remarkably exhibiting very light Higgses and neutralinos (associated with a singlet/singlino component above 90%) and therefore clearly characteristic of the NMSSM. We recall that these are the regions where one expects to find large theoretical predictions for $\sigma_{\tilde{\chi}_1^0-p}$.

On the right-hand side of Fig. 2 we superimpose the results for the $\text{BR}(b \rightarrow s \gamma)$ on the (λ, κ) plane. As discussed in the previous section, the resulting branching ratio is typically large, $\text{BR}(b \rightarrow s \gamma) \gtrsim 3.5 \times 10^{-4}$, and increases to as much as $\sim 5 \times 10^{-4}$ in regions with small κ/λ , where the charged Higgs mass is smaller. Notice therefore that the regions of the (λ, κ) plane associated with larger values of $\text{BR}(b \rightarrow s \gamma)$ typically correspond to those where the largest predictions for $\sigma_{\tilde{\chi}_1^0-p}$ are found. In this example, only a small triangular region with $\lambda \lesssim 0.05$, for $\kappa < 0.7$, is within a 1σ deviation from the experimental bound of Eq. (2.9) and $\lambda \lesssim 0.35$ is needed in order to be within 2σ of that result. In the plot we also indicate with dot-dashed lines the different values of

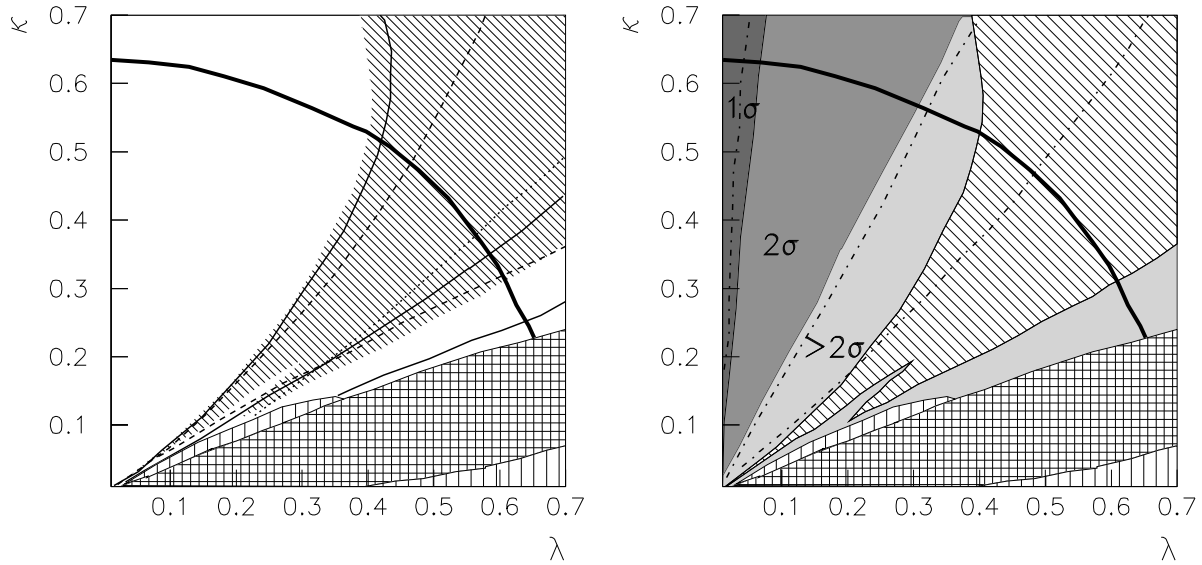


Figure 2: Effect of the experimental constraints on the (λ, κ) plane for an example with $\tan\beta = 3$, $A_\lambda = 200$ GeV, $A_\kappa = -200$ GeV and $\mu = 130$ GeV. In both cases, the gridded area is excluded due to the appearance of tachyons, while the vertically ruled area corresponds to the occurrence of unphysical minima. The oblique ruled area is associated with points that do not satisfy the LEP and/or Tevatron constraints or where (at least) the LEP bound on direct neutralino production is violated. The region above the thick black line is disfavoured due to the occurrence of a Landau pole below the GUT scale. On the left plot, from top to bottom, solid lines indicate different values of the lightest Higgs mass, $m_{h_1^0} = 114, 75, 25$ GeV. Dashed lines separate the regions where the lightest scalar Higgs has a singlet composition given by $S_{13}^2 = 0.1, 0.9$ (from top to bottom). Finally in the area below the dotted line, the lightest neutralino has a singlino composition greater than $N_{15}^2 = 0.1$. On the right, grey areas represent the theoretical predictions for $\text{BR}(b \rightarrow s \gamma)$. From left to right, 1σ (dark), 2σ (medium) and excluded (light) regions are shown. Dot-dashed lines stand for the different values of the charged Higgs mass, $m_{H^\pm} = 1000, 500, 450$ GeV (from left to right).

the charged Higgs mass, thus illustrating the correlation between its decrease and the increase in $\text{BR}(b \rightarrow s \gamma)$.

The effect of the various experimental constraints on the parameter space is very sensitive to variations in the input parameters. We will now investigate how changes in $\tan\beta$ and A_λ affect the resulting $\text{BR}(b \rightarrow s \gamma)$. On the one hand, as already mentioned, increasing the value of $\tan\beta$ leads to a reduction of the charged Higgs contribution.

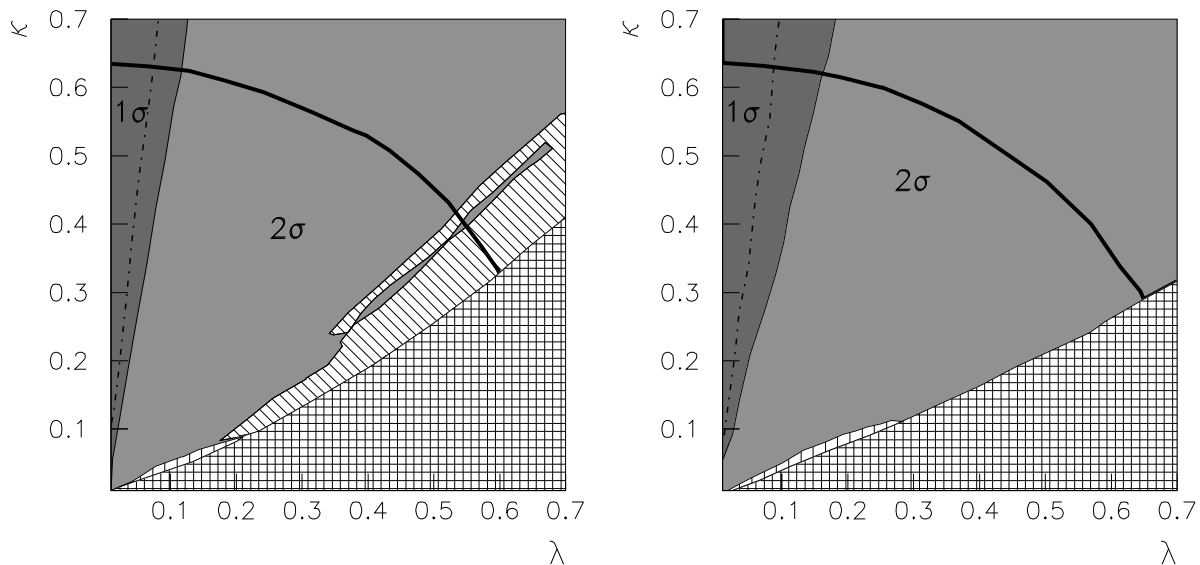


Figure 3: (λ, κ) parameter space for $\tan\beta = 5$, $A_\kappa = -200$ GeV, and $\mu = 130$ GeV. On the left we take $A_\lambda = 200$ GeV, while on the right we consider $A_\lambda = 400$ GeV. Line and colour code follow the conventions of Fig. 2. In this case, the single dot-dashed line corresponds to $m_{H^\pm} = 1000$ GeV.

Since in our case this is the leading contribution to $\text{BR}(b \rightarrow s\gamma)$, an enhancement in $\tan\beta$ enlarges the regions of the parameter space which are consistent with the experimental constraint. This is illustrated on the left-hand side of Fig. 3 with the same example of Fig. 2, but now taking $\tan\beta = 5$. The resulting charged Higgses are heavier ($m_{H^\pm} > 500$ GeV) and as a consequence the entire (λ, κ) plane fulfils the experimental constraint on $\text{BR}(b \rightarrow s\gamma)$. Notice that LEP and Tevatron constraints are also modified. On the other hand, an increase in the trilinear term A_λ also leads to heavier charged Higgses as seen in Eq. (4.14). Therefore, this can induce a further decrease in $\text{BR}(b \rightarrow s\gamma)$. An example of this is shown on the right-hand side of Fig. 3, where in addition to $\tan\beta = 5$, $A_\lambda = 400$ GeV has been used. Again, the whole (λ, κ) plane is allowed due to the increase in m_{H^\pm} .

Let us finally comment on the possibility of changing the signs of μ , A_λ , and A_κ , while keeping $\mu A_\lambda > 0$ and $\mu A_\kappa < 0$. Although the Higgs potential is invariant under this change, the same does not occur for the chargino and neutralino sectors, so that both these spectra, as well as the experimental constraints are likely to be modified. As an illustrative example, we present in Fig. 4 the same case as in the left-hand side of Fig. 3 but with the opposite signs for μ , A_λ , and A_κ . There are some

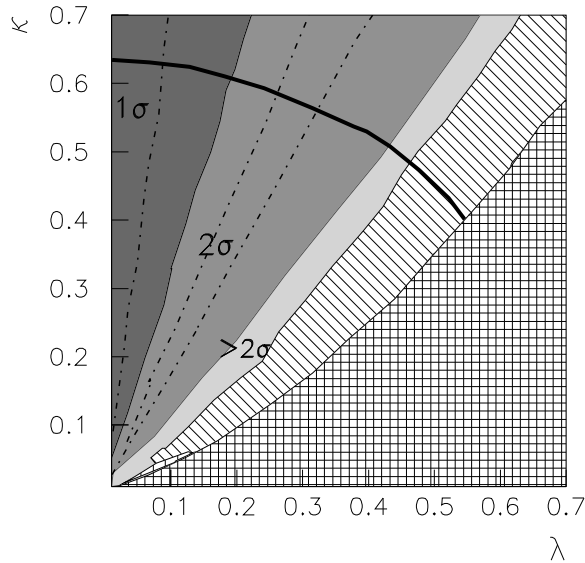


Figure 4: (λ, κ) parameter space for $\tan\beta = 5$, $A_\lambda = -200$ GeV, $A_\kappa = 200$ GeV and $\mu = -130$ GeV. Line and colour code following the conventions of Fig. 2.

important alterations to the areas excluded by unphysical minima and experimental constraints, both of which are now more extensive. Finally, notice that the $\text{BR}(b \rightarrow s \gamma)$ now excludes a larger area of the (λ, κ) plane, thereby disfavouring those areas which potentially lead to larger neutralino detection cross sections.

In the light of this analysis, the optimal areas of the parameter space correspond to those with $\mu, A_\lambda > 0$, and $A_\kappa < 0$, and where $\tan\beta$ and A_λ are relatively large. In order to keep within the context where NMSSM-like dark matter scenarios can be obtained, we will use $\tan\beta \leq 5$.

4.1.2 $\mu A_\kappa < 0$ and $\mu A_\lambda < 0$ ($\kappa > 0$)

Compared to the previous case, the presence of tachyons gives rise to far stronger constraints. Occurring now in both CP-even and CP-odd Higgs sectors, the non-physical (tachyonic) solutions exclude very large areas of the parameter space. Regarding the LEP experimental exclusions, these arise from excessive contributions to $h^0 \rightarrow b\bar{b}$ and $h^0 \rightarrow 2$ jets, and cover an area wider than what had been previously identified in [16] (a consequence of the improved computation of the Higgs spectrum). In addition, due to the lightness of the charged Higgs bosons, an important region is also excluded due to very large $\text{BR}(b \rightarrow s \gamma)$, so that the only surviving regions are those associated with

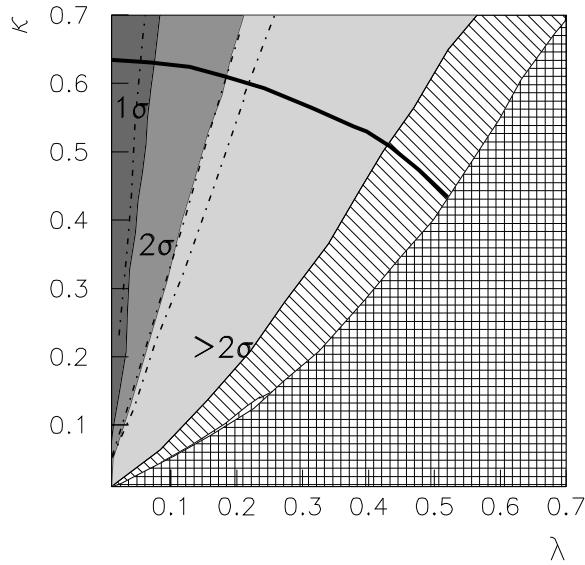


Figure 5: (λ, κ) parameter space for $\tan \beta = 5$, $A_\lambda = -200$ GeV, $A_\kappa = -200$ GeV and $\mu = 130$ GeV. Line and colour code following the conventions of Fig. 2.

$\lambda \lesssim 0.2$. As an example, Fig. 5 displays a case with $\tan \beta = 5$, $A_\lambda = -200$ GeV, $A_\kappa = -200$ GeV and $\mu = 130$ GeV. Let us remark that since the lower-right corner of the (λ, κ) plane is not accessible, one cannot find light neutral Higgs states, so that interesting prospects regarding the direct detection of dark matter should not be expected.

Although varying the several parameters results in modifications of the excluded areas (LEP/Tevatron, $b \rightarrow s \gamma$ and unphysical minima), in all cases these are sizable. Only very reduced regions, corresponding to small values of λ survive all the constraints. In these areas the singlet component of the lightest Higgs is negligible and the lightest neutralino is Higgsino-like, therefore resembling MSSM scenarios. The complementary region, with $A_\lambda, A_\kappa > 0$ and $\mu < 0$, leads to even more extensive tachyonic regions, and we will not further discuss it.

4.1.3 $\mu A_\kappa > 0$ and $\mu A_\lambda > 0$ ($\kappa > 0$)

This combination of signs leads to a parameter space which is plagued with tachyons [16], arising from both Higgs sectors. Contrary to what was noticed for the previous cases, here the unphysical minima occur for small values of λ . The remaining areas in the (λ, κ) plane are also very affected by experimental constraints. As a consequence,

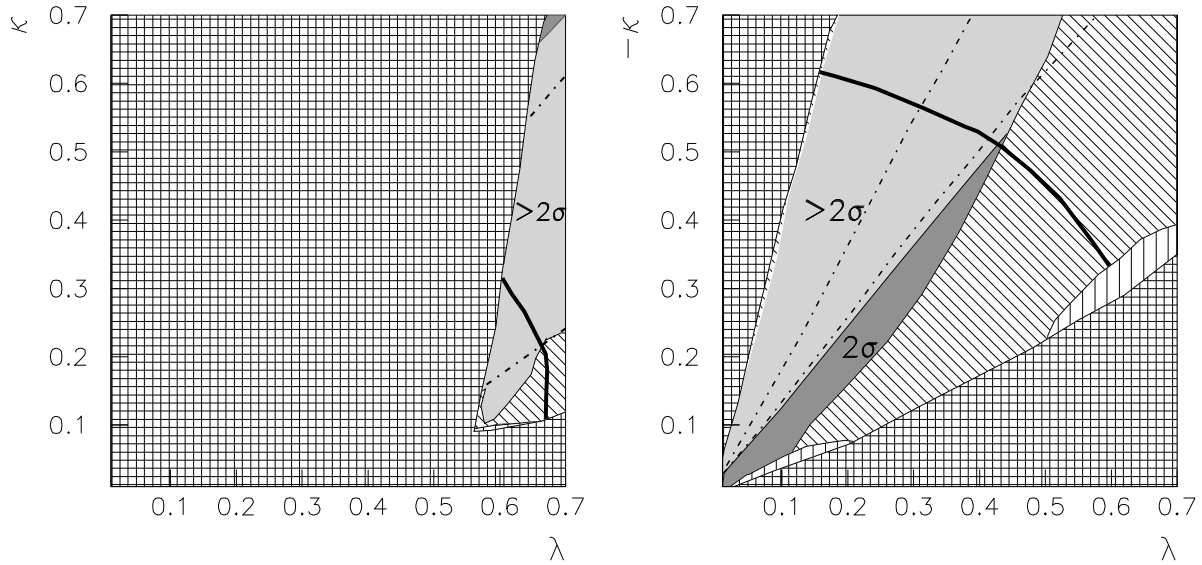


Figure 6: On the left (λ, κ) parameter space for $\tan \beta = 3$, $A_\lambda = 200$ GeV, $A_\kappa = 50$ GeV and $\mu = 160$ GeV. On the right $\tan \beta = 5$, $A_\lambda = 400$ GeV, $A_\kappa = 200$ GeV, and $\mu = 130$ GeV for $\kappa < 0$. Line and colour code following the conventions of Fig. 2.

only very reduced areas of the parameter space survive.

For example, considering the choice $A_\lambda = 200$ GeV, $A_\kappa = 50$ GeV and $\mu = 160$ GeV, with $\tan \beta = 3$, we observe that once the areas corresponding to the occurrence of tachyons are excluded, the small surviving region is still plagued by false minima as well as by the violation of several experimental constraints. In particular, lower values of κ are ruled out due to conflict with LEP ($h^0 \rightarrow b\bar{b}$ and $h^0 \rightarrow 2$ jets) and excessive contributions to the $\text{BR}(b \rightarrow s\gamma)$. This is illustrated on the left-hand side of Fig. 6.

Although reducing the values of A_κ and $\tan \beta$ enlarges the areas where physical minima can be found, the addition of the experimental constraint on $\text{BR}(b \rightarrow s\gamma)$ to the LEP and Tevatron bounds typically rules out the whole (λ, κ) plane. Increasing $\tan \beta$ in order to reduce the contribution to $\text{BR}(b \rightarrow s\gamma)$ is also highly disfavoured since the tachyonic region becomes more important. As a consequence, no interesting implications for neutralino dark matter detection are expected in this case.

4.1.4 $\mu A_\kappa > 0$ and $\mu A_\lambda > 0$ ($\kappa < 0$)

The only viable combination of signs associated with negative values of κ is also plagued by the appearance of tachyons, both in the CP-even and CP-odd Higgs sectors, towards the regions with small λ [16]. In addition, experimental constraints also exclude large portions of the parameter space in the vicinity of the tachyonic regions. As an example, let us mention that for the case $A_\lambda = 100$ GeV, $A_\kappa = 50$ GeV and $\mu = 130$ GeV, with $\tan\beta = 3$, all the parameter space associated with physical minima is ruled out, since either DHDM constraints ($h^0 \rightarrow b\bar{b}$ and $h^0 \rightarrow 2$ jets) are violated or consistency with the $\text{BR}(b \rightarrow s\gamma)$ bound is not achieved. Increasing A_λ , A_κ , and $\tan\beta$ leads to a significant improvement. For example, with $A_\lambda = 400$ GeV, $A_\kappa = 200$ GeV, $\mu = 130$ GeV with $\tan\beta = 5$ some allowed areas are found, as shown on the right-hand side of Fig. 6. Nevertheless, LEP/Tevatron experimental constraints together with the bound on $\text{BR}(b \rightarrow s\gamma)$ rule out those parts of the parameter space where the Higgs is light and more singlet-like, and in which $\sigma_{\tilde{\chi}_1^0-p}$ can be sizable. The remaining allowed regions correspond to a rather small area, in which the lightest Higgs is essentially doublet-like, while the lightest neutralino exhibits a strong Higgsino dominance.

4.2 Neutralino relic density

The next step in our analysis is to take into account the available experimental data on the WIMP relic density. In order to be a viable dark matter candidate, the lightest NMSSM neutralino must have an abundance within the ranges presented in Eqs. (3.11,3.12). Similar to what occurs in the MSSM, this additional constraint further reduces the regions of the low-energy parameter space. Moreover, and as hinted before, one expects that $\Omega_{\tilde{\chi}_1^0} h^2$ will in general lie below the experimental ranges.

A thorough analysis of the relic density of dark matter in the NMSSM has been carried out in [12]. It was found that compatibility with the WMAP constraint is possible in the regions where the lightest Higgs is dominated by the doublet components and the lightest neutralino is a bino-Higgsino mixture. Apart from possible Higgs resonances, compatible values of $\Omega_{\tilde{\chi}_1^0} h^2$ are found for two distinct regions: $\mu \gg M_2$ and $\mu \gtrsim M_1$ (similar to the MSSM for small to intermediate values of $\tan\beta$). Also note that, for regions with $\mu \lesssim M_1$, Higgsino-singlino neutralinos with masses below M_W can give a relic density within the WMAP range (or larger) essentially because the annihilation into Z and W gauge bosons is kinematically forbidden. It is also worth noticing that a pure bino LSP also offers interesting scenarios, with a remarkable

role being played by s -channel Higgs resonances (else $\Omega_{\tilde{\chi}_1^0} h^2$ tends to be above the experimental bound). Additional LSP annihilation via scalar or pseudoscalar Higgses can also play a relevant role.

In order to understand the results for $\Omega_{\tilde{\chi}_1^0} h^2$ one needs to take into account the variations in the mass and composition of the lightest neutralino in the (λ, κ) plane, as well as in the Higgs sector. In general, the neutralino relic density will be too small in those regions of the parameter space where it is Higgsino-like and increases when the neutralino becomes more singlino-like. In addition, one should consider the possible existence of resonant annihilation (when twice the neutralino mass equals the mass of one of the mediating particles in an s -channel) and the kinematic thresholds for the various channels (e.g., annihilations into ZZ , WW , Zh_i^0 , $h_i^0 h_j^0$, $a_i^0 a_j^0$, and $a_i^0 h_j^0$).

Since the goal of our present study is to discuss the potential of NMSSM-like scenarios regarding the theoretical predictions for $\sigma_{\tilde{\chi}_1^0-p}$, in this subsection we focus on those examples of the parameter space having large neutralino detection cross section. We investigate to which extent the inclusion of the bound of the relic density further constrains the parameter space. As pointed out in [16], these scenarios typically occur in association to singlet-like h_1^0 , with singlino-Higgsino neutralinos. Let us study one example in detail.

We begin by taking $M_1 = 160$ GeV, $A_\lambda = 400$ GeV, $A_\kappa = -200$ GeV, and $\mu = 130$ GeV, with $\tan \beta = 5$, which according to Figs. 1 and 3 is consistent with the bounds on a_μ^{SUSY} and $\text{BR}(b \rightarrow s \gamma)$, respectively. The results for the neutralino relic density are depicted in the (λ, κ) plane on the left-hand side of Fig. 7. On the experimentally allowed area, grey dots stand for points which, in addition to experimental constraints, fulfil $0.1 \leq \Omega_{\tilde{\chi}_1^0} h^2 \leq 0.3$, whereas black dots represent points in agreement with the WMAP constraint. Notice that in this case, no points are excluded by LEP or Tevatron bounds.

For large values of κ and small λ (i.e., on the upper left corner of the plots), the lightest neutralino is relatively heavy and has a mixed bino-Higgsino composition, since we have chosen $\mu \sim M_1$. Due to the large Higgsino component, the neutralino relic density is very small, and cannot account for the observed amount of dark matter. As we move in the (λ, κ) plane towards smaller values of κ and larger values of λ , the neutralino becomes lighter and has a larger singlino component (in this example $N_{15}^2 \lesssim 0.35$), and as a consequence, $\Omega_{\tilde{\chi}_1^0} h^2$ increases. As the neutralino mass decreases, some annihilation channels become kinematically forbidden, such as annihilation into a pair of Z or W bosons when $m_{\tilde{\chi}_1^0} < M_Z$ or $m_{\tilde{\chi}_1^0} < M_W$, respectively. We have indicated

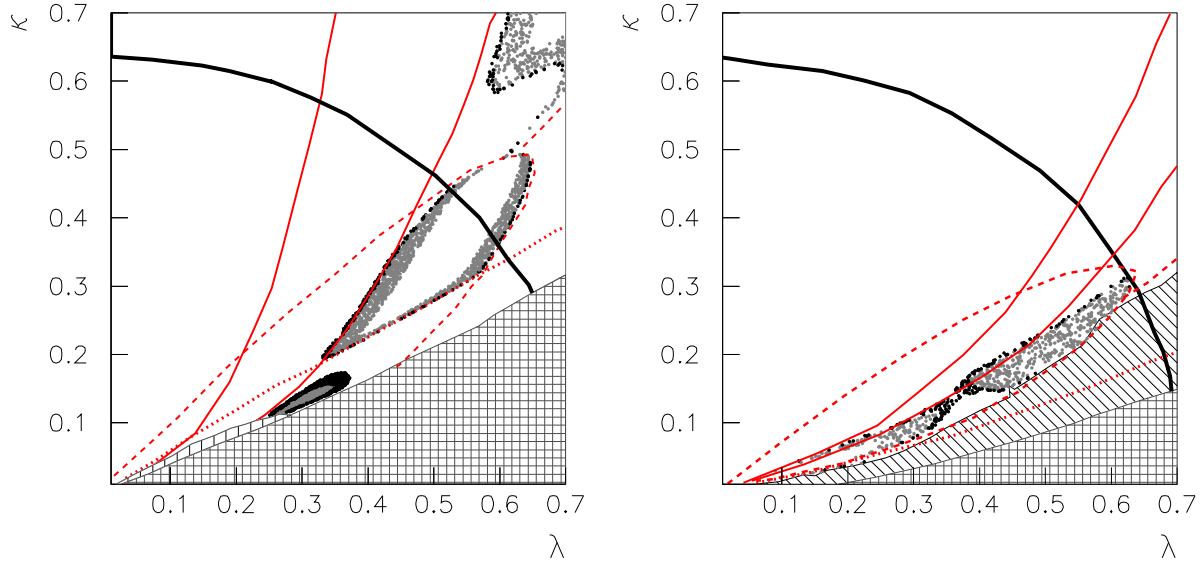


Figure 7: (λ, κ) parameter space with information about the neutralino relic density. On the left, an example with $M_1 = 160$ GeV, $\tan \beta = 5$, $A_\lambda = 400$ GeV, $A_\kappa = -200$ GeV, and $\mu = 130$ GeV. The gridded area is excluded due to the appearance of tachyons, while the vertically ruled area corresponds to the occurrence of unphysical minima. The region above the thick black line is disfavoured because of the occurrence of a Landau pole below the GUT scale. The oblique ruled area is associated to those points that do not satisfy LEP/Tevatron and/or $\text{BR}(b \rightarrow s \gamma)$ constraints, whereas the bound on a_μ^{SUSY} is fulfilled in the whole plane. The dark shaded (cyan) area corresponds to points which are experimentally viable, and whose relic density complies with the astrophysical bound of Eq. (3.11). Points in black are those in agreement with experimental constraints and WMAP bounds (c.f. Eq. (3.12)). The dashed red lines indicate the resonances of the lightest neutralino annihilation channels through the second lightest CP-even Higgs, $2m_{\tilde{\chi}_1^0} = m_{h_2^0}$. In the region below the red dotted line the lightest neutralino mass is larger than the mass of the lightest Higgs. Along the red solid lines the neutralino mass is equal to the Z and W mass (from left to right, respectively). On the right, the same example is shown, but with $A_\kappa = 0$ and $\mu = 150$ GeV.

these two thresholds in the figure with red solid lines. Below these the resulting relic density can be large enough to fulfil the WMAP constraint. Variations in the Higgs sector also affect the calculation of the neutralino abundance. On the one hand, the mass and composition of the lightest Higgs also vary throughout the (λ, κ) plane. Lighter Higgses with a larger singlet composition are obtained for small values of κ . In our case, $m_{\tilde{\chi}_1^0} < m_{h_1^0}$ for large κ and small λ , but eventually, the Higgs becomes lighter and new annihilation channels (the most important being $\tilde{\chi}_1^0 \tilde{\chi}_1^0 \rightarrow h_1^0 h_1^0$ and $Z h_1^0$) are available for the neutralino, thus decreasing its relic density. The points where $m_{\tilde{\chi}_1^0} = m_{h_1^0}$ are indicated with a dotted red line in the plot. On the other hand, one also needs to take into account the existence of rapid neutralino annihilation with the second-lightest CP-even Higgs, when $2m_{\tilde{\chi}_1^0} = m_{h_2^0}$, which is responsible for a further decrease in $\Omega_{\tilde{\chi}_1^0} h^2$. This is indicated in the plot with a red dashed line.

As we can see, in the present example the correct relic density is only obtained when either the singlino composition of the neutralino is large enough or when the annihilation channels into Z , W , or h_1^0 are kinematically forbidden. Interestingly, some allowed areas are very close to the tachyonic border. The neutralino-nucleon cross section can be very large in these regions, due to the presence of very light singlet-like Higgses (in this example $S_{13}^2 \approx 0.99$).

The same example, but now with $A_\kappa = 0$ and $\mu = 150$ GeV is shown on the right-hand side of Fig. 7. Once more, in order to reproduce the correct $\Omega_{\tilde{\chi}_1^0} h^2$ the neutralino has to be either sufficiently light so that some annihilations channels are closed or have a large singlino component. In this particular case the singlino component of $\tilde{\chi}_1^0$ can be even larger, with $N_{15}^2 \sim 0.9$ in the allowed area with very low κ . Notice, however, that the region in the vicinity of the tachyonic area is excluded by experimental bounds.

In order to study the importance of the neutralino composition, we will now consider variations in the gaugino masses. To begin with, we increase the bino mass and take $M_1 = 330$ GeV, thereby decreasing the bino component of the lightest neutralino. Such an increase of the gaugino masses implies a reduced contribution to the muon anomalous magnetic moment. We obtain $a_\mu^{\text{SUSY}} \approx 7.2 \times 10^{-10}$ (see Fig. 1), more than 2σ away from the central value and therefore disfavoured. The resulting (λ, κ) plane is represented on the left-hand side of Fig. 8. Since the Higgsino component has increased with respect to the previous examples, the resulting relic density for the neutralino in the region with large κ and small λ is even smaller. Once more, in order to have the correct $\Omega_{\tilde{\chi}_1^0} h^2$ we need to go to regions of the parameter space where some annihilation channels are not kinematically allowed and/or the neutralino is singlino-like. Notice

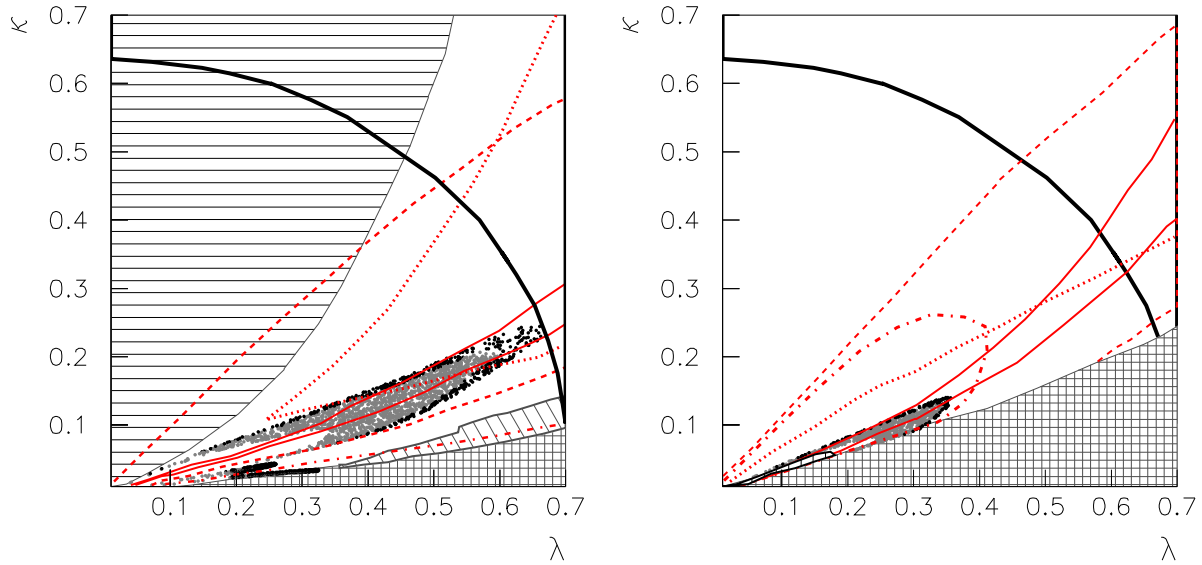


Figure 8: On the left, the same as in Fig. 7 but with $M_1 = 330$ GeV, $\tan \beta = 5$, $A_\lambda = 570$ GeV, $A_\kappa = -60$ GeV, with $\mu = 160$ GeV. The area to the right of the red dotted line has $m_{\tilde{\chi}_1^0} < m_{h_1^0}$. Along the red dot-dashed line, $2m_{\tilde{\chi}_1^0} = M_Z$, leading to rapid neutralino annihilation. On the right, the same with $M_1 = 500$ GeV, $\tan \beta = 5$, $A_\lambda = 400$ GeV, $A_\kappa = -150$ GeV, with $\mu = 130$ GeV. In this example the red dot-dashed line indicates resonances on the neutralino annihilation mediated by the lightest pseudoscalar when $2m_{\tilde{\chi}_1^0} = m_{a_1^0}$. In both examples the resulting a_μ^{SUSY} is outside the experimental 2σ region.

also that the neutralino is in general heavier in this example and therefore the lines with $m_{\tilde{\chi}_1^0} = M_Z$ and $m_{\tilde{\chi}_1^0} = M_W$ are shifted to lower values of κ . Also, the region with $m_{\tilde{\chi}_1^0} < m_{h_1^0}$ is modified and now corresponds to the area on the right of the dotted red line. Finally, we must take into account the possible resonances along which $\Omega_{\tilde{\chi}_1^0} h^2$ decreases. In this example, rapid annihilation of neutralinos occurs via CP-even Higgs exchange when $2m_{\tilde{\chi}_1^0} = m_{h_1^0}$, which takes place along the two upper red dashed lines. There is also a resonance with the Z boson when $2m_{\tilde{\chi}_1^0} = M_Z$ which occurs along the lower red dashed line. It is worth noticing that, once more, a part of the region allowed by experimental and astrophysical constraints lies close to the tachyonic area, and could have a large $\sigma_{\tilde{\chi}_1^0-p}$.

Finally on the right-hand side of Fig. 8 we show another example where the bino mass has been further increased to $M_1 = 500$ GeV. The contribution to the muon anomalous magnetic moment is also too low. As shown in Fig. 1, $a_\mu^{\text{SUSY}} \approx 4 \times 10^{-10}$,

more than 2σ away from the experimental value. Due to the further increase of the Higgsino component and mass of the lightest neutralino, its relic density is even smaller and compatibility with WMAP is only obtained when the neutralino is lighter than the lightest Higgs and, at least, the W boson. Notice that in this example there is also a resonant annihilation through the lightest CP-odd Higgs when $2m_{\tilde{\chi}_1^0} \approx m_{a_1^0}$, which further decreases $\Omega_{\tilde{\chi}_1^0} h^2$. This constrains the allowed region to small values of λ , in which the neutralino is mostly singlino, $N_{15}^2 \lesssim 0.8$.

To summarise, in these scenarios, neutralinos typically have a very small relic density (insufficient to account for the dark matter in the Universe) as a consequence of their large Higgsino composition. Only when one moves towards regions of the parameter space where the singlino composition is enhanced or the neutralino mass is decreased (such that some annihilation channels become forbidden) can the WMAP result be reproduced.

We have not yet addressed the other areas of the parameter space (ii)-(iv). These other choices of signs for the different parameters are associated to less favourable scenarios. First, in cases (ii) and (iv) the experimental constraints rule out the regions where $\tilde{\chi}_1^0$ has a large singlino component. Therefore, the lightest neutralino is in general Higgsino-like throughout all the allowed (λ, κ) plane and, consequently, its relic abundance is much below the favoured values, i.e., $\Omega_{\tilde{\chi}_1^0} h^2 \ll 0.1$. In case (iii), where large areas are excluded because of the occurrence of tachyons, it is extremely complicated to find regions that simultaneously fulfil the experimental and astrophysical constraints. For this reason, in the following section we will limit our analysis to case (i).

As a next step of our analysis, we will bring together all the constraints so far explored, and after having ensured that we are indeed in the presence of a viable NMSSM scenario (namely with the correct relic density), we will investigate to which extent the lightest neutralino can be detectable in dark matter experiments.

4.3 Neutralino direct detection prospects

After having discussed the new and the improved constraints on the low-energy parameter space, we will now address whether or not NMSSM neutralinos with a relic density in agreement with current limits are likely to be detected by the present or the next generation of dark matter detectors.

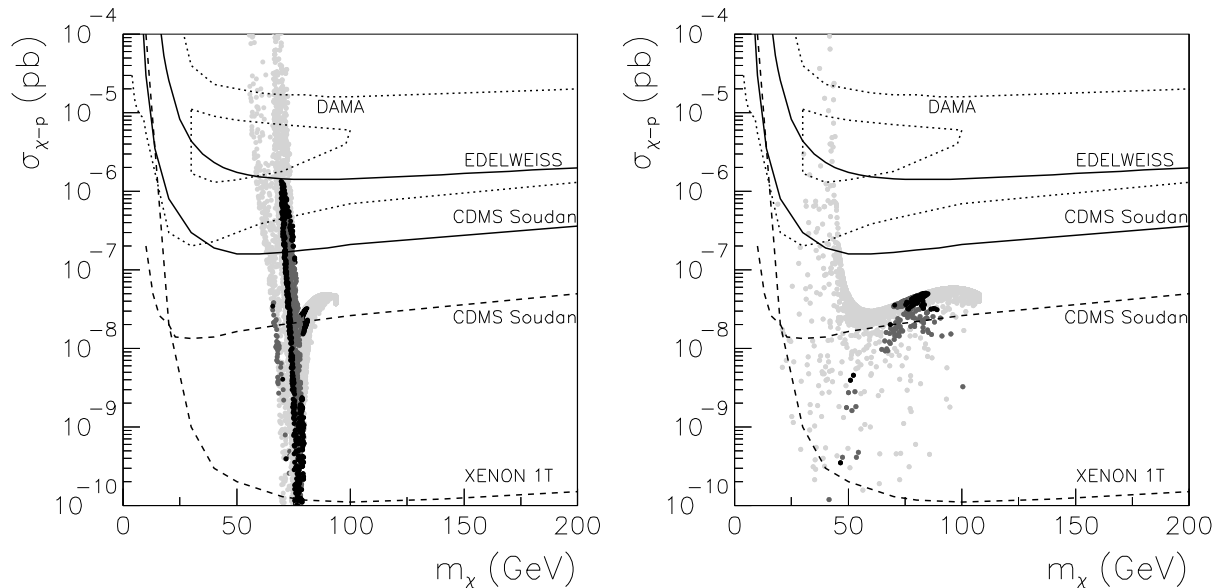


Figure 9: Scatter plot of the scalar neutralino-nucleon cross section as a function of the lightest neutralino mass. On the left, an example with $M_1 = 160$ GeV, $\tan\beta = 5$, $A_\lambda = 400$ GeV, $A_\kappa = -200$ GeV, and $\mu = 130$ GeV. All the points represented are in agreement with LEP/Tevatron, a_μ^{SUSY} , and $\text{BR}(b \rightarrow s\gamma)$ bounds. Dark gray dots represent points which, in addition, fulfil $0.1 \leq \Omega_{\tilde{\chi}_1^0} h^2 \leq 0.3$, whereas black dots are those in agreement with the WMAP constraint. The sensitivities of present and projected experiments are also depicted, with solid and dashed lines, respectively. On the right we show the same example but with $\mu = 150$ GeV and $A_\kappa = 0$.

Although in our survey of the low-energy NMSSM parameter space we have scanned over all combinations of signs (i)-(iv), as we already mentioned, cases (ii)-(iv) present far less interesting situations regarding the neutralino relic density. Even though one can find in the latter three cases some challenging situations regarding direct detection prospects [16], the new imposed constraints imply that finding experimentally viable areas, with a sizable $\sigma_{\tilde{\chi}_1^0-p}$, becomes nearly impossible. Thus, for the present study we will focus on case (i). We will go through the same examples as in the previous subsection.

Let us start with the regime where $M_1 \approx \mu$, and as an example ensuring compatibility with WMAP, choose $A_\lambda = 400$ GeV, $A_\kappa = -200$ GeV, $\mu = 130$ GeV, with $\tan\beta = 5$ (corresponding to what was already depicted on the right panel of Fig. 3 and the left of Fig. 7). As shown in the previous subsection, there exist regions in the parameter space where the neutralino fulfils all experimental constraints and has the correct relic

density. The latter are characterised by neutralinos with a significant singlino fraction and/or a small mass. In this case, one of the allowed regions is close to the tachyonic area and exhibits very light singlet-like Higgses, potentially leading to large detection cross sections. This is indeed the case, as evidenced on the left-hand side of Fig. 9, where the theoretical predictions for $\sigma_{\tilde{\chi}_1^0-p}$ are plotted versus the lightest neutralino mass. The resulting $\sigma_{\tilde{\chi}_1^0-p}$ spans several orders of magnitude, but, remarkably, areas with $\sigma_{\tilde{\chi}_1^0-p} \gtrsim 10^{-7}$ pb are found. These correspond to the above mentioned regions of the parameter space with very light singlet-like Higgses ($25 \text{ GeV} \lesssim m_{h_1^0} \lesssim 50 \text{ GeV}$ with $S_{13}^2 \gtrsim 0.99$). The neutralino is a mixed singlino-Higgsino state with $N_{15}^2 \approx 0.35$ and a mass around 75 GeV.

The sensitivities of present and projected dark matter experiments are also depicted for comparison. The small area bounded by dotted lines is allowed by the DAMA experiment in the simple case of an isothermal spherical halo model [17]. The larger area also bounded by dotted lines represents the DAMA region when uncertainties to this simple model are taken into account [18]. For the other experiments in the figure only the spherical halo has been considered in their analyses. In particular, the (upper) areas bounded by solid lines are excluded by EDELWEISS [21] ⁶ and CDMS Soudan [20]. Finally, the dashed lines represent the sensitivities of the projected CDMS Soudan and XENON 1T [23] experiments.

On the right-hand side of Fig. 9 we show the resulting $\sigma_{\tilde{\chi}_1^0-p}$ when the μ parameter and A_κ are varied to $\mu = 150 \text{ GeV}$, $A_\kappa = 0$, for which the effect of the different constraints on the (λ, κ) plane were represented on the right-hand side of Fig. 7. Since the areas of the parameter space with very light Higgses are ruled out by experimental constraints the detection cross section is not as large as in the previous examples. In the regions consistent with both experimental and astrophysical constraints the lightest Higgs mass is in the range $80 \text{ GeV} \lesssim m_{h_1^0} \lesssim 120 \text{ GeV}$, thus leading to $\sigma_{\tilde{\chi}_1^0-p} \lesssim 5 \times 10^{-8}$ pb, within the sensitivity of projected dark matter experiments, such as CDMS Soudan.

Let us now investigate the effect of changing the neutralino composition by modifying the bino mass. As commented in [16], the largest values of the neutralino detection cross section were obtained for a mixed singlino-Higgsino composition, when $\mu \lesssim M_1 < M_2$. In order to enhance the Higgsino composition we will consider examples where M_1 is increased with respect to the μ -parameter. Such neutralinos annihilate

⁶Since the exclusion area due to ZEPLIN I [22] is similar to EDELWEISS we have not depicted it here, nor in any subsequent plot.

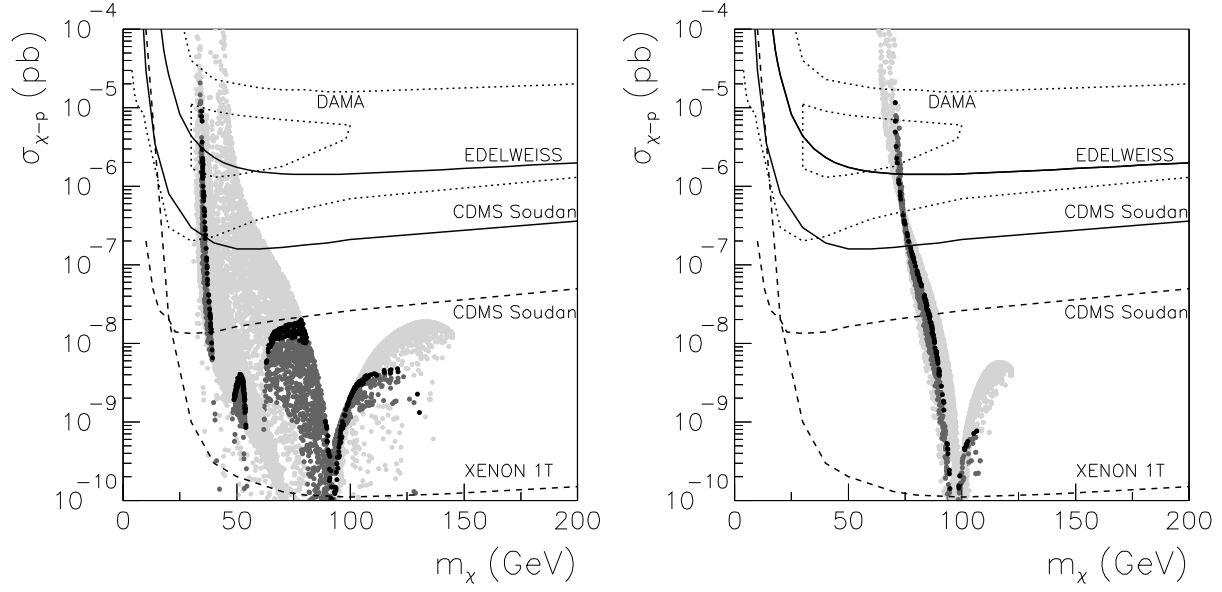


Figure 10: The same as in Fig.9 but for an example with $M_1 = 330$ GeV, $\tan\beta = 5$, $A_\lambda = 570$ GeV, $A_\kappa = -60$ GeV, with $\mu = 160$ GeV (left) and $M_1 = 500$ GeV, $\tan\beta = 5$, $A_\lambda = 400$ GeV, $A_\kappa = -150$ GeV, with $\mu = 130$ GeV (right). In both examples, the resulting a_μ^{SUSY} is outside the experimental 2σ region.

more efficiently, thus leading to a reduced $\Omega_{\tilde{\chi}_1^0} h^2$, so that the astrophysical constraint becomes more stringent. Nevertheless, as seen in the previous subsection, it is still possible to find areas of the parameter space with the correct relic density while simultaneously fulfilling all experimental constraints. These regions corresponded to light singlet-like Higgses, which can potentially lead to sizable detection cross sections.

First, $M_1 = 330$ GeV will be taken, for an example with $\mu = 160$ GeV, $A_\lambda = 570$ GeV, $A_\kappa = -60$ GeV, and $\tan\beta = 5$. The parameter space for this case was represented in Fig. 8, where we showed the effect of resonant annihilation channels on the allowed regions. The theoretical predictions for neutralino direct detection are shown in Fig. 10. In this plot, the various resonances appear as funnels in the predicted $\sigma_{\tilde{\chi}_1^0-p}$ for the regions with the correct $\Omega_{\tilde{\chi}_1^0} h^2$ at the corresponding values of the neutralino mass ($m_{\tilde{\chi}_1^0} \approx M_Z/2$ and $m_{\tilde{\chi}_1^0} \approx m_{h_1^0}/2$). Below the resonance with the Z boson, light neutralinos are obtained $m_{\tilde{\chi}_1^0} \lesssim M_Z/2$ with a large singlino composition which have the correct relic abundance. The lightest Higgs is also singlet-like and very light, leading to a very large detection cross section, $\sigma_{\tilde{\chi}_1^0-p} \gtrsim 10^{-6}$ pb. This corresponds to the allowed area of the (λ, κ) plane which lies in the vicinity of the tachyonic region in

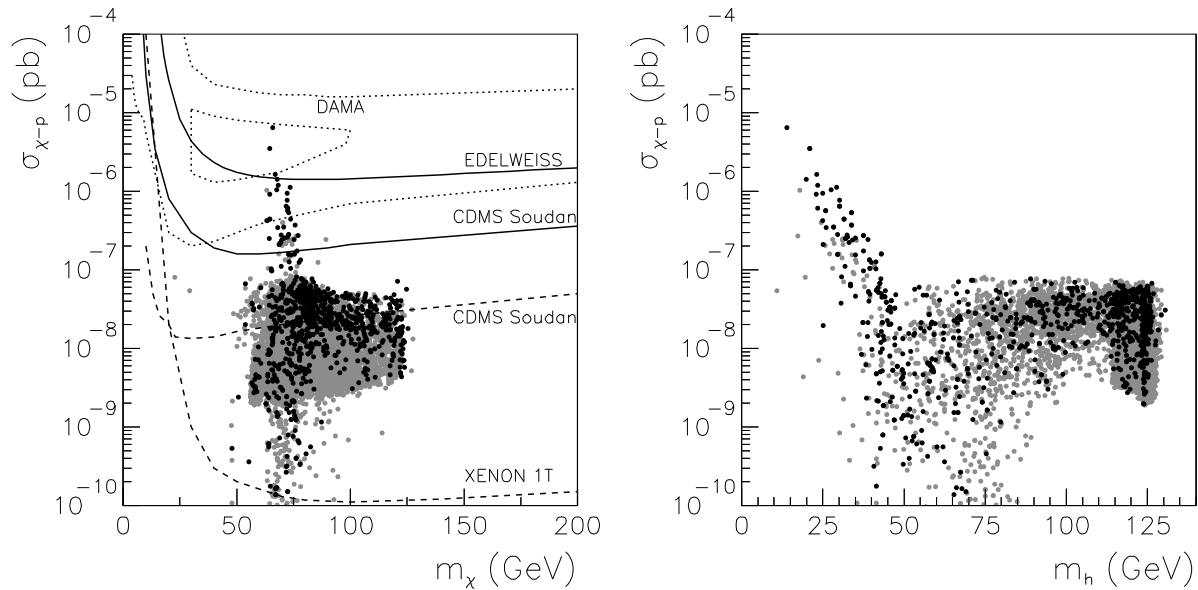


Figure 11: Scatter plot of the neutralino-nucleon cross section as a function of the neutralino mass (left) and as a function of the lightest CP-even Higgs mass (right) for an example with $\tan\beta = 5$, and the remaining parameters in the ranges $0.01 \leq \lambda, \kappa \leq 0.7$, $110 \text{ GeV} \lesssim M_2 \lesssim 430 \text{ GeV}$, $-300 \text{ GeV} \lesssim A_\kappa \lesssim 300 \text{ GeV}$, $-800 \text{ GeV} \lesssim A_\lambda \lesssim 800 \text{ GeV}$, and $110 \text{ GeV} < \mu < 300 \text{ GeV}$. All the points represented are in agreement with LEP/Tevatron, a_μ^{SUSY} , and $\text{BR}(b \rightarrow s\gamma)$ constraints, and have a relic density in agreement with the astrophysical bound (grey dots) or the WMAP constraint (black dots).

Fig. 8.

Remember however that these two examples with a larger bino mass were disfavoured by the resulting muon anomalous magnetic moment, as it was illustrated in Fig. 1.

One more example, this time for $M_1 = 500 \text{ GeV}$, $\mu = 130 \text{ GeV}$, $A_\lambda = 400 \text{ GeV}$, $A_\kappa = -150 \text{ GeV}$, and $\tan\beta = 5$ is represented in Fig. 10 and shows how large detection cross sections can also be achieved for heavier neutralinos. In this case (whose parameter space was illustrated and discussed in Fig. 8) neutralino detection cross sections as large as $\sigma_{\tilde{\chi}_1^0-p} \approx 10^{-5} \text{ pb}$ are possible while fulfilling experimental and astrophysical constraints. Once more, the occurrence of light singlet-like Higgses is crucial for enhancing $\sigma_{\tilde{\chi}_1^0-p}$ and the sizable singlino component of the lightest neutralino ($N_{15}^2 \approx 0.9$) reduces the annihilation cross section and ensures the correct relic density.

Finally, we show in Fig. 11 a scatter plot of the theoretical predictions for the

neutralino-nucleon cross section as a function of the neutralino mass and the lightest Higgs mass when λ , κ , M_1 , the μ parameter and the trilinear terms, A_λ and A_κ are varied while keeping $\tan\beta = 5$. In order to satisfy the a_μ^{SUSY} constraint, a small slepton mass, $m_{L,E} = 150$ GeV, has been used. Only the points which are in agreement with LEP/Tevatron, $\text{BR}(b \rightarrow s\gamma)$, and a_μ^{SUSY} limits and which, in addition, are consistent with the astrophysical bound or the WMAP constraint on the relic density are plotted. We clearly see how large detection cross sections are correlated to the presence of very light Higgses ($m_{h_1^0} \lesssim 50$ GeV). Neutralinos fulfilling all constraints and within the reach of dark matter experiments are possible with $50 \text{ GeV} \lesssim m_{\tilde{\chi}_1^0} \lesssim 130 \text{ GeV}$. The upper bound on the neutralino mass is due to the lightest stau becoming the LSP. If the slepton mass is increased, heavier neutralinos can be found but the resulting a_μ^{SUSY} is soon outside the experimentally allowed range.

5 Conclusions

We have extended the systematic analysis started in [16] of the low-energy parameter space of the Next-to-Minimal Supersymmetric Standard Model (NMSSM), studying the implications of experimental and astrophysical constraints on the direct detection of neutralino dark matter. We have computed the theoretical predictions for the scalar neutralino-proton cross section, $\sigma_{\tilde{\chi}_1^0-p}$, and compared it with the sensitivities of present and projected dark matter experiments. In the computation we have taken into account all available experimental bounds from LEP and Tevatron, including constraints coming from B and K physics, as well as the supersymmetric contribution to the muon anomalous magnetic moment, a_μ^{SUSY} . Finally, the relic abundance of neutralinos has also been computed and consistency with astrophysical constraints imposed.

We have found very stringent constraints on the parameter space coming from low-energy observables. On the one hand, a_μ^{SUSY} is generally very small unless very light slepton ($m_{L,E} \lesssim 200$ GeV) and gaugino masses ($M_1 \lesssim 210$ GeV) are considered, and slepton trilinear couplings modified in order to increase the LR mixing in the smuon mass matrix. On the other hand, the contribution to $\text{BR}(b \rightarrow s\gamma)$ is sizable, mostly due to the smallness of the charged Higgs mass, so that regions with $\tan\beta \lesssim 3$ are disfavoured.

Regarding the neutralino relic density, regions of the parameter space can be found where $\Omega_{\tilde{\chi}_1^0} h^2$ is in agreement with the WMAP constraint. This is possible when either

the neutralino mass is small enough for some annihilation channels to be kinematically forbidden or when the singlino component of the lightest neutralino is large enough to suppress neutralino annihilation.

Remarkably, some of the regions fulfilling all the experimental and astrophysical constraints display very light Higgses, $m_{h_1^0} \sim 50$ GeV, which are singlet-like, $S_{13}^2 \gtrsim 0.9$, thus allowing a sizable increase of the neutralino-nucleon cross section. Neutralinos with a detection cross-section within the reach of dark matter experiments are therefore possible, and have a mass in the range $50 \text{ GeV} \lesssim m_{\tilde{\chi}_1^0} \lesssim 130 \text{ GeV}$. These neutralinos have a mixed singlino-Higgsino composition and are therefore characteristic of the NMSSM.

Acknowledgements

D. G. Cerdeño is supported by the program “Juan de la Cierva” of the Ministerio de Educación y Ciencia of Spain. The work of E. Gabrielli was supported by the Academy of Finland (Project number 104368). The work of C. Muñoz was supported in part by the Spanish DGI of the MEC under Proyecto Nacional FPA2006-05423, by the European Union under the RTN program MRTN-CT-2004-503369, and under the ENTApP Network of the ILIAS project RII3-CT-2004-506222. Likewise, the work of D. G. Cerdeño, D. E. López-Fogliani, and C. Muñoz, was also supported in part by the Spanish DGI of the MEC under Proyecto Nacional FPA2006-01105 and under Acción Integrada Hispano-Francesa HF-2005-0005, and by the Comunidad de Madrid under Proyecto HEPHACOS, Ayudas de I+D S-0505/ESP-0346. The work of A. M. Teixeira was supported by the French ANR project PHYS@COL&COS.

References

- [1] H. Goldberg, “Constraint on the photino mass from cosmology,” *Phys. Rev. Lett.* **50** (1983) 1419;
 J. R. Ellis, J. S. Hagelin, D. V. Nanopoulos and M. Srednicki, “Search For Supersymmetry At The Anti-P P Collider,” *Phys. Lett. B* **127** (1983) 233;
 L. M. Krauss, “New Constraints On ‘Ino’ Masses From Cosmology. 1. Supersymmetric ‘Inos’,” *Nucl. Phys. B* **227** (1983) 556;

- J. R. Ellis, J. S. Hagelin, D. V. Nanopoulos, K. A. Olive and M. Srednicki, “Supersymmetric relics from the big bang,” Nucl. Phys. B **238** (1984) 453.
- [2] For a review see, C. Muñoz, “Dark matter detection in the light of recent experimental results,” Int. J. Mod. Phys. A **19** (2004) 3093 [arXiv:hep-ph/0309346].
- [3] P. Fayet, “Supergauge invariant extension of the Higgs mechanism and a model for the electron and its neutrino,” Nucl. Phys. B **90** (1975) 104;
R. K. Kaul and P. Majumdar, “Cancellation of quadratically divergent mass corrections in globally supersymmetric spontaneously broken gauge theories,” Nucl. Phys. B **199** (1982) 36;
R. Barbieri, S. Ferrara and C. A. Savoy, “Gauge models with spontaneously broken local supersymmetry,” Phys. Lett. B **119** (1982) 343;
H. P. Nilles, M. Srednicki and D. Wyler, “Weak interaction breakdown induced by supergravity,” Phys. Lett. B **120** (1984) 346;
J. M. Frere, D. R. T. Jones and S. Raby, “Fermion masses and induction of the weak scale by supergravity,” Nucl. Phys. B **222** (1983) 11;
J. P. Derendinger and C. A. Savoy, “Quantum effects and $SU(2)\times U(1)$ breaking in supergravity gauge theories,” Nucl. Phys. B **237** (1984) 307.
- [4] J.E. Kim and H.P. Nilles, “The μ problem and the strong CP problem,” Phys. Lett. B **138** (1984) 150.
- [5] M. Bastero-Gil, C. Hugonie, S. F. King, D. P. Roy and S. Vempati, “Does LEP prefer the NMSSM?,” Phys. Lett. B **489** (2000) 359 [arXiv:hep-ph/0006198].
- [6] J. R. Ellis, J. F. Gunion, H. E. Haber, L. Roszkowski and F. Zwirner, “Higgs bosons in a nonminimal supersymmetric model,” Phys. Rev. D **39** (1989) 844.
M. Drees, “Supersymmetric models with extended Higgs sector,” Int. J. Mod. Phys. A **4** (1989) 3635;
U. Ellwanger, M. Rausch de Traubenberg and C. A. Savoy, “Particle spectrum in supersymmetric models with a gauge singlet,” Phys. Lett. B **315** (1993) 331 [arXiv:hep-ph/9307322]; “Phenomenology of supersymmetric models with a singlet,” Nucl. Phys. B **492** (1997) 21 [arXiv:hep-ph/9611251];
S. F. King and P. L. White, “Resolving the constrained minimal and next-to-minimal supersymmetric standard models,” Phys. Rev. D **52** (1995) 4183 [arXiv:hep-ph/9505326].

- [7] U. Ellwanger and C. Hugonie, “Topologies of the (M+1)SSM with a singlino LSP at LEP2,” *Eur. Phys. J. C* **13** (2000) 681 [arXiv:hep-ph/9812427].
- [8] U. Ellwanger and C. Hugonie, “Masses and couplings of the lightest Higgs bosons in the (M+1)SSM,” *Eur. Phys. J. C* **25** (2002) 297 [arXiv:hep-ph/9909260].
- [9] U. Ellwanger, J. F. Gunion and C. Hugonie, “NMHDECAY: A Fortran code for the Higgs masses, couplings and decay widths in the NMSSM,” *JHEP* **0502** (2005) 066 [arXiv:hep-ph/0406215].
- [10] U. Ellwanger, J. F. Gunion, C. Hugonie and S. Moretti, “NMSSM Higgs discovery at the LHC,” arXiv:hep-ph/0401228.
- [11] B. R. Greene and P. J. Miron, “Supersymmetric cosmology with a gauge singlet,” *Phys. Lett. B* **168** (1986) 226;
R. Flores, K. A. Olive and D. Thomas, “A new dark matter candidate in the minimal extension of the supersymmetric standard model,” *Phys. Lett. B* **245** (1990) 509;
K. A. Olive and D. Thomas, “A light dark matter candidate in an extended supersymmetric model,” *Nucl. Phys. B* **355** (1991) 192;
S. A. Abel, S. Sarkar and I. B. Whittingham, “Neutralino dark matter in a class of unified theories,” *Nucl. Phys. B* **392** (1993) 83 [arXiv:hep-ph/9209292];
A. Stephan, “Dark matter constraints on the parameter space and particle spectra in the nonminimal SUSY standard model,” *Phys. Lett. B* **411** (1997) 97 [arXiv:hep-ph/9704232]; “Dark matter constraints in the minimal and nonminimal SUSY standard model,” *Phys. Rev. D* **58** (1998) 035011 [arXiv:hep-ph/9709262];
A. Menon, D. E. Morrissey and C. E. M. Wagner, “Electroweak baryogenesis and dark matter in the nMSSM,” *Phys. Rev. D* **70** (2004) 035005 [arXiv:hep-ph/0404184].
- [12] G. Belanger, F. Boudjema, C. Hugonie, A. Pukhov and A. Semenov, “Relic density of dark matter in the NMSSM,” *JCAP* **0509** (2005) 001 [arXiv:hep-ph/0505142].
- [13] J. F. Gunion, D. Hooper and B. McElrath, “Light neutralino dark matter in the NMSSM,” *Phys. Rev. D* **73** (2006) 015011 [arXiv:hep-ph/0509024].
- [14] R. Flores, K. A. Olive and D. Thomas, “Light-neutralino interactions in matter in an extended supersymmetric standard model,” *Phys. Lett. B* **263** (1991) 425.

- [15] V. A. Bednyakov and H. V. Klapdor-Kleingrothaus, “About direct dark matter detection in next-to-minimal supersymmetric standard model”, *Phys. Rev. D* **59** (1999) 023514 [arXiv:hep-ph/9802344].
- [16] D. G. Cerdeño, C. Hugonie, D. E. López-Fogliani, C. Muñoz and A. M. Teixeira, “Theoretical predictions for the direct detection of neutralino dark matter in the NMSSM,” *JHEP* **0412** (2004) 048 [arXiv:hep-ph/0408102].
- [17] DAMA Collaboration, R. Bernabei et al., “Search for WIMP annual modulation signature: results from DAMA/NaI-3 and DAMA/NaI-4 and the global combined analysis”, *Riv. Nuovo Cim.* **26N1** (2003) 1 [arXiv:astro-ph/0307403].
- [18] P. Belli, R. Cerulli, N. Fornengo and S. Scopel, “Effect of the galactic halo modeling on the DAMA/NaI annual modulation result: an extended analysis of the data for WIMPs with a purely spin-independent coupling,” *Phys. Rev. D* **66** (2002) 043503 [arXiv:hep-ph/0203242].
- [19] P. Ullio, M. Kamionkowski and P. Vogel, “Spin-dependent WIMPs in DAMA?,” *JHEP* **0107** (2001) 044 [arXiv:hep-ph/0010036];
D. Smith and N. Weiner, “Inelastic dark matter”, *Phys. Rev. D* **64** (2001) 043502 [arXiv:hep-ph/0101138]; “Inelastic dark matter at DAMA, CDMS and future experiments,” talk given at DM 2002 Conference, Marina del Rey, California (2002), arXiv:astro-ph/0208403;
R. Bernabei et al., “Investigating the DAMA annual modulation data in the framework of inelastic dark matter,” *Eur. Phys. J. C* **23** (2002) 61;
G. Prezeau, A. Kurylov, M. Kamionkowski and P. Vogel, “New contribution to WIMP-nucleus scattering,” *Phys. Rev. Lett.* **91** (2003) 231301 [arXiv:astro-ph/0309115];
C. Savage, P. Gondolo and K. Freese, “Can WIMP spin dependent couplings explain DAMA data, in the light of null results from other experiments?,” *Phys. Rev. D* **70** (2004) 123513 [arXiv:astro-ph/0408346].
- [20] D. S. Akerib et al. [CDMS Collaboration], “First results from the cryogenic dark matter search in the Soudan Underground Lab,” *Phys. Rev. Lett.* **93** (2004) 211301 [arXiv:astro-ph/0405033].
- [21] EDELWEISS Collaboration, A. Benoit et al., “First results of the EDELWEISS WIMP search using a 320-g heat-and-ionization Ge detector,” *Phys. Lett. B* **513**

- (2001) 15 [arXiv:astro-ph/0106094]; “Improved exclusion limits from the EDELWEISS WIMP search,” Phys. Lett. B **545** (2002) 43 [arXiv:astro-ph/0206271].
- [22] G. J. Alner et al. [UK Dark Matter Collaboration], “First limits on nuclear recoil events from the ZEPLIN I galactic dark matter detector,” Astropart. Phys. **23** (2005) 444.
- [23] See e.g., E. Aprile et al., “The XENON dark matter search experiment,” Nucl. Phys. Proc. Suppl. **138** (2005) 156 [arXiv:astro-ph/0407575].
- [24] U. Ellwanger and C. Hugonie, “NMHDECAY 2.0: An updated program for sparticle masses, Higgs masses, couplings and decay widths in the NMSSM,” Comput. Phys. Commun. **175**, 290 (2006) [arXiv:hep-ph/0508022].
- [25] G. Belanger, F. Boudjema, A. Pukhov and A. Semenov, “MicrOMEGAs: A program for calculating the relic density in the MSSM,” Comput. Phys. Commun. **149** (2002) 103 [arXiv:hep-ph/0112278]; “MicrOMEGAs: Version 1.3,” Comput. Phys. Commun. **174** (2006) 577 [arXiv:hep-ph/0405253].
- [26] LEPSUSYWG, ALEPH, DELPHI, L3, OPAL experiments, note LEPSUSYWG/4-01.1 and 04-02.1 (<http://lepsusy.web.cern.ch/lepsusy/Welcome.html>); LEP Higgs Working Group for Higgs boson searches Collaboration, “Search for charged Higgs bosons: Preliminary combined results using LEP data collected at energies up to 209-GeV,” arXiv:hep-ex/0107031.
- [27] T. Affolder et al. [CDF Collaboration], “Search for gluinos and scalar quarks in $p\bar{p}$ collisions at $\sqrt{s} = 1.8$ -TeV using the missing energy plus multijets signature,” Phys. Rev. Lett. **88** (2002) 041801 [arXiv:hep-ex/0106001];
B. Abbott et al. [D0 Collaboration], “Search for squarks and gluinos in events containing jets and a large imbalance in transverse energy,” Phys. Rev. Lett. **83** (1999) 4937 [arXiv:hep-ex/9902013].
- [28] W. M. Yao et al. [Particle Data Group], “Review of particle physics,” J. Phys. G **33** (2006) 1.
- [29] DELPHI Collaboration, J. Abdallah et al., “Searches for supersymmetric particles in e^+e^- collisions up to 208 GeV and interpretation of the results within the MSSM,” Eur. Phys. J. C **31** (2004) 421 [arXiv:hep-ex/0311019];
OPAL Collaboration, G. Abbiendi et al., “Search for chargino and neutralino

- production at $\sqrt{s} = 192 \text{ GeV} - 209 \text{ GeV}$ at LEP,” *Eur. Phys. J. C* **35** (2004) 1 [arXiv:hep-ex/0401026].
- [30] LEP Higgs Working Group for Higgs boson searches Collaboration, R. Barate et al., “Search for the standard model Higgs boson at LEP,” *Phys. Lett. B* **565** (2003) 61 [arXiv:hep-ex/0306033];
 OPAL Collaboration, G. Abbiendi et al., “Decay-mode independent searches for new scalar bosons with the OPAL detector at LEP,” *Eur. Phys. J. C* **27** (2003) 311 [arXiv:hep-ex/0206022]; “Flavour independent search for Higgs bosons decaying into hadronic final states in e^+e^- collisions at LEP,” *Phys. Lett. B* **597** (2004) 11 [arXiv:hep-ex/0312042];
 LEP Higgs Working Group for Higgs boson searches Collaboration, “Flavor independent search for hadronically decaying neutral Higgs bosons at LEP,” arXiv:hep-ex/0107034; “Searches for Higgs bosons decaying into photons: combined results from the LEP experiments,” LHWG Note/2002-02; “Searches for invisible Higgs bosons: Preliminary combined results using LEP data collected at energies up to 209 GeV,” arXiv:hep-ex/0107032;
 ALEPH Collaboration, D. Buskulic et al., “Search for a nonminimal Higgs boson produced in the reaction $e^+e^- \rightarrow hZ^*$,” *Phys. Lett. B* **313** (1993) 312;
 DELPHI Collaboration, “Search for Neutral Higgs Bosons in Extended Models,” CERN EP 2003-061 (submitted to EPJ).
- [31] G. Hiller, “b-physics signals of the lightest CP-odd Higgs in the NMSSM at large $\tan(\beta)$,” *Phys. Rev. D* **70** (2004) 034018 [arXiv:hep-ph/0404220].
- [32] K. Adel and Y.P. Yao, “Exact α_s calculation of $b \rightarrow s + \gamma$ $b \rightarrow s + g$,” *Phys. Rev. D* **49** (1994) 4945 [arXiv:hep-ph/9308349];
 A. Ali and C. Greub, “Photon energy spectrum in $B \rightarrow X(s) + \gamma$ and comparison with data,” *Phys. Lett. B* **361**(1995) 146 [arXiv:hep-ph/9506374];
 M. Misiak and M. Münz, “Two loop mixing of dimension five flavor changing operators,” *Phys. Lett. B* **344** (1995) 308 [arXiv:hep-ph/9409454];
 C. Greub, T. Hurth, and D. Wyler, “Virtual $O(\alpha_s)$ corrections to the inclusive decay $b \rightarrow s\gamma$,” *Phys. Rev. D* **54** (1996) 3350 [arXiv:hep-ph/9603404];
 C. Greub and T. Hurth, “Two-loop matching of the dipole operators for $b \rightarrow s\gamma$ and $b \rightarrow sg$,” *Phys. Rev. D* **56** (1997) 2934 [arXiv:hep-ph/9703349];
 N. Pott, “Bremsstrahlung corrections to the decay $b \rightarrow s\gamma$,” *Phys. Rev. D* **54** (1996) 938 [arXiv:hep-ph/9512252];

- K. G. Chetyrkin, M. Misiak and M. Munz, “Weak radiative B-meson decay beyond leading logarithms,” *Phys. Lett. B* **400** (1997) 206 [Erratum-ibid. *B* **425** (1998) 414] [arXiv:hep-ph/9612313];
- A. J. Buras, A. Kwiatkowski and N. Pott, “Next-to-leading order matching for the magnetic photon penguin operator in the $B \rightarrow X_s \gamma$ decay,” *Nucl. Phys. B* **517** (1998) 353 [arXiv:hep-ph/9710336];
- A. J. Buras, A. Czarnecki, M. Misiak and J. Urban, “Completing the NLO QCD calculation of $\bar{B} \rightarrow X_s \gamma$,” *Nucl. Phys. B* **631** (2002) 219 [arXiv:hep-ph/0203135].
- [33] P. Gambino and M. Misiak, “Quark mass effects in $\bar{B} \rightarrow X_s \gamma$,” *Nucl. Phys. B* **611** (2001) 338 [arXiv:hep-ph/0104034].
- [34] A. L. Kagan and M. Neubert, “QCD anatomy of $B \rightarrow X_s \gamma$ decays,” *Eur. Phys. J. C* **7**, 5 (1999) [arXiv:hep-ph/9805303].
- [35] S. Bertolini, F. Borzumati, A. Masiero and G. Ridolfi, “Effects of supergravity induced electroweak breaking on rare B decays and mixings,” *Nucl. Phys. B* **353** (1991) 591.
- [36] M. Ciuchini, G. Degrassi, P. Gambino and G. F. Giudice, “Next-to-leading QCD corrections to $B \rightarrow X_s \gamma$: Standard model and two-Higgs doublet model,” *Nucl. Phys. B* **527** (1998) 21 [arXiv:hep-ph/9710335]; “Next-to-leading QCD corrections to $B \rightarrow X_s \gamma$ in supersymmetry,” *Nucl. Phys. B* **534** (1998) 3 [arXiv:hep-ph/9806308];
- P. Ciafaloni, A. Romanino and A. Strumia, “Two-loop QCD corrections to charged-Higgs-mediated $b \rightarrow s \gamma$ decay,” *Nucl. Phys. B* **524** (1998) 361 [arXiv:hep-ph/9710312];
- F. Borzumati and C. Greub, “2HDMs predictions for $\bar{B} \rightarrow X_s \gamma$ in NLO QCD,” *Phys. Rev. D* **58** (1998) 074004 [arXiv:hep-ph/9802391]; “Two Higgs doublet model predictions for $\bar{B} \rightarrow X_s \gamma$ in NLO QCD. (Addendum),” *Phys. Rev. D* **59** (1999) 057501 [arXiv:hep-ph/9809438];
- G. Degrassi, P. Gambino and G. F. Giudice, “ $B \rightarrow X_s \gamma$ in supersymmetry: Large contributions beyond the leading order,” *JHEP* **0012** (2000) 009 [arXiv:hep-ph/0009337];
- M. Carena, D. Garcia, U. Nierste and C. E. M. Wagner, “ $b \rightarrow s \gamma$ and supersymmetry with large $\tan \beta$,” *Phys. Lett. B* **499** (2001) 141 [arXiv:hep-ph/0010003];
- F. Borzumati, C. Greub and Y. Yamada, “Beyond leading-order corrections to

- $\bar{B} \rightarrow X_s \gamma$ at large $\tan \beta$: The charged-Higgs contribution,” Phys. Rev. D **69**, 055005 (2004) [arXiv:hep-ph/0311151].
- [37] The Heavy Flavour Averaging Group, <http://www.slac.stanford.edu/xorg/hfag/>;
 J. Walsh for the BaBar Collaboration, talk presented at Moriond EW, 2005;
 P. Koppenburg et al. [Belle Collaboration], “An inclusive measurement of the photon energy spectrum in $b \rightarrow s \gamma$ decays,” Phys. Rev. Lett. **93** (2004) 061803 [arXiv:hep-ex/0403004];
 S. Chen et al. [CLEO Collaboration], “Branching fraction and photon energy spectrum for $b \rightarrow s \gamma$,” Phys. Rev. Lett. **87** (2001) 251807 [arXiv:hep-ex/0108032].
- [38] P. Gambino, “Semileptonic and radiative B decays circa 2005,” Nucl. Phys. Proc. Suppl. **156** (2006) 169 [arXiv:hep-ph/0510085] (Talk given at 10th Int. Conference on B Physics at Hadron Machines (BEAUTY 2005), Assisi, Perugia, Italy, 20-24 Jun 2005).
- [39] J. L. Lopez, D. V. Nanopoulos and X. Wang, “Large $(g - 2)_\mu$ in $SU(5) \times U(1)$ supergravity models,” Phys. Rev. D **49** (1994) 366 [arXiv:hep-ph/9308336];
 U. Chattopadhyay and P. Nath, “Probing supergravity grand unification in the Brookhaven $g - 2$ experiment,” Phys. Rev. D **53** (1996) 1648 [arXiv:hep-ph/9507386];
 T. Moroi, “The Muon Anomalous Magnetic Dipole Moment in the Minimal Supersymmetric Standard Model,” Phys. Rev. D **53** (1996) 6565 [Erratum-ibid. D **56** (1997) 4424] [arXiv:hep-ph/9512396];
 M. Carena, G. F. Giudice and C. E. M. Wagner, “Constraints on supersymmetric models from the muon anomalous magnetic moment,” Phys. Lett. B **390** (1997) 234 [arXiv:hep-ph/9610233].
- [40] T. Kinoshita and W.J. Marciano, in *Quantum Electrodynamics*, ed. T. Kinoshita (World Scientific, Singapore, 1990), p. 419;
 T. Kinoshita, “New value of the α^3 electron anomalous magnetic moment,” Phys. Rev. Lett. **75** (1995) 4728;
 A. Czarnecki, B. Krause and W. J. Marciano, “Electroweak corrections to the muon anomalous magnetic moment,” Phys. Rev. Lett. **76** (1996) 3267 [arXiv:hep-ph/9512369];
 S. Eidelman and F. Jegerlehner, “Hadronic contributions to $g - 2$ of the leptons and to the effective fine structure constant $\alpha(M_Z^2)$,” Z. Phys. C **67** (1995) 585 [arXiv:hep-ph/9502298];

- K. Adel and F. J. Yndurain, “Improved evaluation of the hadronic vacuum polarization contributions to muon $g - 2$ and $\bar{\alpha}_{\text{QED}}(M_Z)$ using high order QCD calculations,” arXiv:hep-ph/9509378;
- T. Kinoshita, B. Nizic and Y. Okamoto, “Hadronic Contributions To The Anomalous Magnetic Moment Of The Muon,” Phys. Rev. D **31** (1985) 2108;
- J. Bijmns, E. Pallante and J. Prades, “Hadronic light by light contributions to the muon $g - 2$ in the large $N(c)$ limit,” Phys. Rev. Lett. **75** (1995) 1447 [Erratum-ibid. **75** (1995) 3781] [arXiv:hep-ph/9505251].
- [41] M. Davier, S. Eidelman, A. Hocker and Z. Zhang, “Updated estimate of the muon magnetic moment using revised results from e^+e^- annihilation,” Eur. Phys. J. C **31** (2003) 503 [arXiv:hep-ph/0308213];
- K. Hagiwara, A. D. Martin, D. Nomura and T. Teubner, “Predictions for $g - 2$ of the muon and $\alpha_{\text{QED}}(M_Z^2)$,” Phys. Rev. D **69** (2004) 093003 [arXiv:hep-ph/0312250];
- J. F. de Troconiz and F. J. Yndurain, “The hadronic contributions to the anomalous magnetic moment of the muon,” Phys. Rev. D **71** (2005) 073008 [arXiv:hep-ph/0402285].
- [42] T. Kinoshita and M. Nio, “The tenth-order QED contribution to the lepton $g - 2$: Evaluation of dominant α^5 terms of muon $g - 2$,” Phys. Rev. D **73** (2006) 053007 [arXiv:hep-ph/0512330];
- K. Hagiwara, A. D. Martin, D. Nomura and T. Teubner, “Improved predictions for $g - 2$ of the muon and $\alpha_{\text{QED}}(M_Z^2)$,” arXiv:hep-ph/0611102.
- [43] G. W. Bennett et al. [Muon $g-2$ Collaboration], “Measurement of the negative muon anomalous magnetic moment to 0.7-ppm,” Phys. Rev. Lett. **92** (2004) 161802 [arXiv:hep-ex/0401008].
- [44] For a review, see M. Persic, P. Salucci and F. Stel, “The Universal rotation curve of spiral galaxies: 1. The Dark matter connection,” Mon. Not. Roy. Astron. Soc. **281** (1996) 27 [arXiv:astro-ph/9506004];
- Y. Sofue and V. Rubin, “Rotation Curves of Spiral Galaxies,” Ann. Rev. Astron. Astrophys. **39** (2001) 137 [arXiv:astro-ph/0010594];
- M. Roncadelli, “Searching for dark matter,” arXiv:astro-ph/0307115;
- P. Salucci and M. Persic, “Dark Matter Halos around Galaxies,” arXiv:astro-ph/9703027;

- E. Battaner and E. Florido, “The rotation curve of spiral galaxies and its cosmological implications,” *Fund. Cosmic Phys.* **21** (2000) 1 [arXiv:astro-ph/0010475].
- [45] W. L. Freedman, “Determination of cosmological parameters,” *Phys. Scripta* **T85** (2000) 37 [arXiv:astro-ph/9905222].
- [46] D. N. Spergel et al., ”Wilkinson Microwave Anisotropy Probe (WMAP) Three Year Results: Implications for Cosmology,” arXiv:astro-ph/0603449;
C. L. Bennett et al., “First Year Wilkinson Microwave Anisotropy Probe (WMAP) observations: Preliminary maps and basic results,” *Astrophys. J. Suppl.* **148** (2003) 1 [arXiv:astro-ph/0302207];
D. N. Spergel et al. [WMAP Collaboration], “First Year Wilkinson Microwave Anisotropy Probe (WMAP) observations: Determination of cosmological parameters,” *Astrophys. J. Suppl.* **148** (2003) 175 [arXiv:astro-ph/0302209];
L. Verde et al., “First Year Wilkinson Microwave Anisotropy Probe (WMAP) observations: Parameter estimation methodology”, *Astrophys. J. Suppl.* **148** (2003) 195 [arXiv:astro-ph/0302218].